AD-A062 763 OREGON GRADUATE CENTER BEAVERTON DEPT OF APPLIED PHY--ETC F/G 4/1
STRONG OPTICAL SCATTERING IN ATMOSPHERIC TURBULENCE.(U)
SEP 78 R A ELLIOTT, J R KERR, P A PINCUS AFOSR-77-3401
AFOSR-TR-78-1519 NL

UNCLASSIFIED

| OF |
AD
A062763

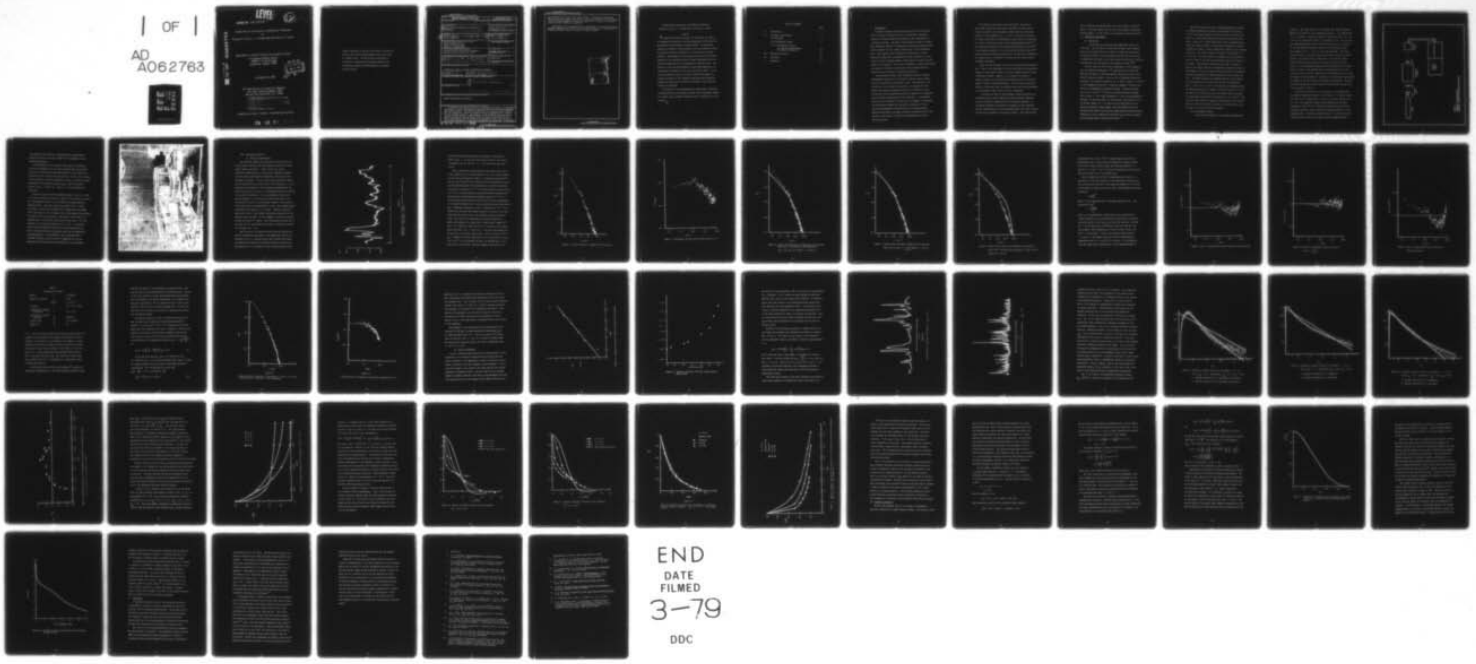

END
DATE
FILMED
3-79
DDC

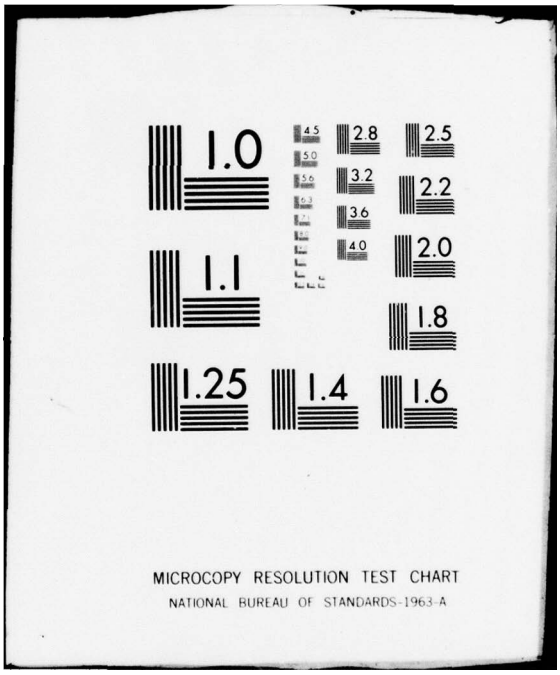
1.0
1.1
1.25
1.4
1.6
1.8
2.0
2.2
2.5
2.8
3.2
3.6
4.0
4.5
5.0
5.6
6.3
MICROCOPY RESOLUTION TEST CHART
NATIONAL BUREAU OF STANDARDS-1963-A

AFOSR-TR- 78-1519

Strong Optical Scattering in Atmospheric Turbulence

BY

Richard A. Elliott, J. Richard Kerr and Philip A. Pincus

Department of Applied Physics & Electronic Science
The Oregon Graduate Center
19600 N. W. Walker Road
Beaverton, Oregon 97005

September 30, 1978

Air Force Office of Scientific Research
Air Force Systems Command, USAF
Bolling Air Force Base, D.C. 20332

Research sponsored by the Air Force Office of Scientific Research, Air Force Systems Command, USAF, under Grant No. AFOSR-77-3401. The United States Government is authorized to reproduce and distribute reprints for Governmental purposes notwithstanding any copyright notation hereon.

Unclassified

SECURITY CLASSIFICATION OF THIS PAGE *(When Data Entered)*

REPORT DOCUMENTATION PAGE

READ INSTRUCTIONS BEFORE COMPLETING FORM

1. REPORT NUMBER

2. GOVT ACCESSION NO.

3. RECIPIENT'S CATALOG NUMBER

4. TITLE *(and Subtitle)*

(16) Strong Optical Scattering in Atmospheric Turbulence

5. TYPE OF REPORT & PERIOD COVERED

Final report. Aug 1, '77 to July 31, '78

6. PERFORMING ORG. REPORT NUMBER

7. AUTHOR(s)

(10) Richard A. Elliott, J. Richard Kerr and Philip A. Pincus

8. CONTRACT OR GRANT NUMBER(s)

(15) AFOSR-77-3401

9. PERFORMING ORGANIZATION NAME AND ADDRESS

Oregon Graduate Center
19600 N. W. Walker Road
Beaverton, Oregon 97005

10. PROGRAM ELEMENT, PROJECT, TASK AREA & WORK UNIT NUMBERS

11. CONTROLLING OFFICE NAME AND ADDRESS

Air Force Office of Scientific Research
Bolling Air Force Base, D.C. 20332

12. REPORT DATE

September 30, 1978

13. NUMBER OF PAGES

54

14. MONITORING AGENCY NAME & ADDRESS *(if different from Controlling Office)*

(11) 30 Sep 78 (12) 60 p.

15. SECURITY CLASS. *(of this report)*

Unclassified

15a. DECLASSIFICATION/DOWNGRADING SCHEDULE

16. DISTRIBUTION STATEMENT *(of this Report)*

Approved for public release; distribution unlimited.

(18) AFOSR (19) TR-78-1519

17. DISTRIBUTION STATEMENT *(of the abstract entered in Block 20, if different from Report)*

(9) Final rept. 1 Aug 77-31 Jul 78,

18. SUPPLEMENTARY NOTES

19. KEY WORDS *(Continue on reverse side if necessary and identify by block number)*

Optical Scattering, Turbulence

20. ABSTRACT *(Continue on reverse side if necessary and identify by block number)*

A versatile and useful facility for simulating the effects of atmospheric turbulence on optical propagation is described and the relevant system parameters characterized. The scattering medium is a turbulent liquid (ethanol) with the turbulence created by unstable convection generated by a strong vertical thermal gradient. Measurements of the structure function and the spatial spectrum of the resulting refractive index fluctuations are presented and compared with the theoretically predicted forms. The effects of this scattering medium on laser beam propagation are determined (continued)

DD FORM 1 JAN 73 1473 EDITION OF 1 NOV 65 IS OBSOLETE

Unclassified

SECURITY CLASSIFICATION OF THIS PAGE *(When Data Entered)*

and compared to the first order Rytov theory. In particular probability density functions, moments and spatial covariance functions of the irradiance resulting from propagation through the system with a variety of turbulence levels and path lengths are presented.

The results of an investigation into generating a controlled scattering medium by dispersing uniformly sized transparent spheres in a medium with a slightly different index of refraction is also reported.

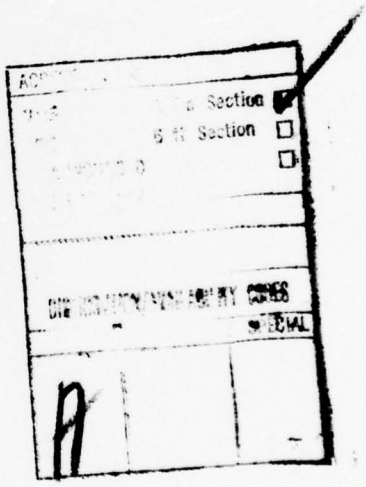

Strong Optical Scattering in Atmospheric Turbulence

Richard A. Elliott, J. Richard Kerr, and Philip A. Pincus

Abstract

A versatile and useful facility for simulating the effects of atmospheric turbulence on optical propagation is described and the relevant system parameters characterized. The scattering medium is a turbulent liquid (ethanol) with the turbulence created by unstable convection generated by a strong vertical thermal gradient. Measurements of the structure function and the spatial spectrum of the resulting refractive index fluctuations are presented and compared with the theoretically predicted forms. The effects of this scattering medium on laser beam propagation are determined and compared to the first order Rytov theory. In particular probability density functions, moments and spatial covariance functions of the irradiance resulting from propagation through the system with a variety of turbulence levels and path lengths are presented.

The results of an investigation into generating a controlled scattering medium by dispersing uniformly sized transparent spheres in a medium with a slightly different index of refraction is also reported.

TABLE OF CONTENTS

I. Introduction

A one-year program in modeling optical scattering from atmospheric turbulence through the use of a controllable, repeatable laboratory scattering medium has resulted in the establishment of a versatile facility. The goal of this program has been to investigate fundamental aspects of transitional and strong scattering under conditions which are not readily achieved over a real atmospheric path. These aspects, which include the verification of recent analytical predictions, are important for the confident use of the Green's function (Huygens-Fresnel) formulations for complex sources, targets, and scenarios. The current re-emphasis of shorter-wavelength (as opposed to infrared) systems gives these strong-scattering questions direct relevance to systems applications.

The deleterious effects that propagation through a randomly inhomogeneous medium has on an initially coherent optical signal can only be described in statistical terms. The probability distribution of the irradiance fluctuations, its moments, and the spatial and temporal covariance functions are examples of quantities which can be measured and which are important for designing optical systems operating under such conditions. A considerable effort has been expended in recent years in attempts to understand the relationship between the statistical properties of the irradiance and measurable characteristics of the random medium. These characteristics are again statistical properties such as the variance of the index of refraction inhomogeneities and their spatial spectrum.

The results of this effort have been mixed. The Rytov or first order theory[1] has been highly successful for weak scattering and relatively short propagation paths, where the normalized variance of the irradiance $\sigma_I^2 << 1$, but it is entirely erroneous for longer paths where the experimental results show σ_I^2 saturating to a value of order unity rather than increasing monotonically.[2-4] More modern works based on the extended Huygen-Fresnel principle[5-7] or approximate solutions for the fourth order coherence function[8,9] have certainly elucidated the problem but the analytical expressions are complex and it is difficult to obtain precise results without extensive computation.

There are also problems involved in obtaining good experimental data. Most of the experimental work has been done in the atmosphere because of the potential impact on optical communication and target illumination systems. However, it is difficult to realize a uniform, stable, well characterized propagation path of sufficient length to generate strong scattering. For this reason some model system or alternative type of scatterer that would allow experiments in the laboratory under precise control is desirable.

It has been the goal of this program to obtain definitive experimental results under conditions allowing detailed comparison with the theoretical predictions and to determine empirical relationships between the statistical parameters of the irradiance and the random medium for those situations which still defy analysis. Our work has proceeded in two parallel efforts. One involves work

with an improved and refined version of recent efforts on scattering by a turbulent liquid, and the other uses randomly distributed uniform spheres. We will report on the turbulent liquid work first.

II. Turbulent Liquid Medium

(i) Background

In the past year there has been significant activity in this field. On the analytical side Hill has made a more complete study of the spatial spectrum of index of refraction fluctuations in turbulent fluids. He has considered not only fluctuations due to temperature variations in air and liquids but also due to humidity fluctuations in air and salinity fluctuations in water.[10,11]

From our point of view the most significant of his findings is that the ubiquitous Kolmogorov $\kappa^{-5/3}$ spectrum does not adequately describe the index of refraction spatial spectrum but must be modified at high wave numbers. That is, the -5/3 inertial-convective subrange of the spectrum extends up to $\kappa \approx (10\eta)^{-1}$, where $\eta = (\nu^3/\epsilon)^{1/4}$ is the Kolmogorov microscale, ν being the kinematic viscosity and ϵ the rate of dissipation of mechanical energy. Beyond this point and up to $\kappa \approx (Pr)^{1/2}\ \eta^{-1}$ there is a viscous-convective subrange with a slope -1. For higher wavenumbers, in the viscous-dissipative subrange, the spectrum falls off exponentially. The quantity Pr is the Prandtl number, $Pr = \nu/D$, where D is the diffusivity of the quantity causing the index change. Hill and Clifford have also calculated the effect this spectral change induces in the statistical properties of the irradiance and show that it can often be significant including cases of practical interest.[12]

There have also been recent, relevant experiments performed on laboratory generated turbulence by Bissonette[13] and Gurvich et al.[14] Both groups heated a liquid from below and studied the effect on a laser beam propagating through the convective turbulence. The use of a liquid rather than a gas is advantageous because the change in index of refraction with temperature (dn/dt) is greater by several orders of magnitude, leading to much stronger scattering. The Prandtl number of liquids is also higher (Pr = 0.7 for air, 7 for water and 16 for ethanol) so the one would expect the "bump" in the spectrum predicted by Hill and Clifford to be larger. Unfortunately the Russian group made no attempt to measure the spatial spectrum of temperature fluctuations directly but assumed a form for the spectrum and determined the parameters involved by measuring the thermal gradient and flux through the cell. Bissonette measured the temporal spectrum of the temperature fluctuations and the structure function of temperature, $D_T(r) = \langle |T(\underline{r} + \underline{r}_1) - T(\underline{r}_1)|^2 \rangle$, and reported no disagreement with the Kolmogorov spectrum. However, since there was no net flow of the water in his scattering tank, the inferred spatial spectrum is questionable because Taylor's hypothesis is not valid.[15] Also, the probes with which the temperature fluctuations were recorded could not resolve scale sizes less than 2 mm, while scale sizes as small as 1 mm may very well be present.

(ii) Experimental System

The scattering apparatus is illustrated schematically

in Fig. 1. The light source is a 50 mW HeNe laser (Spectra Physics Model 125) followed by a beam expanding telescope. A collimated beam 1.2 cm in diameter propagates through the scattering cell, a 25 × 25 × 50 cm tank filled with ethanol, at a height of 14 cm. For multiple pass experiments mirrors can be inserted to provide up to 5 passes of the beam through independent regions of the turbulent liquid. Path lengths of 0.5, 1.5 and 2.5 m are thus available. The light leaving the cell is projected onto the detection system of 16 photodiodes in two linear arrays of eight each. The effective interdiode spacing and aperture size is controlled by the projection optics. In the experiments described below the aperture size ranged from 53 to 500 μm. The minimum distance between diodes was varied from 92 to 875 μm with the largest effective separation being 6.13 mm. The signals from the diodes are recorded by a microprocessor-controlled 16 channel 14 bit A/D converter and digital tape recorder. The data collection system has a dynamic range of 80 dB and the sampling rate can be as great as 200 Hz.

Turbulence was created in the scattering cell by maintaining an unstable temperature gradient in the ethanol. The tank is heated from below by an aluminum plate resting on electrical heaters rated at 1 kW. The temperature gradient was maintained and the mean temperature controlled by circulating thermostatically-controlled cold water through a copper tubing heat exchanger resting on a flat aluminum plate 1 cm below the liquid surface. In order to prevent large convection cells from forming vertical plexiglas dividers

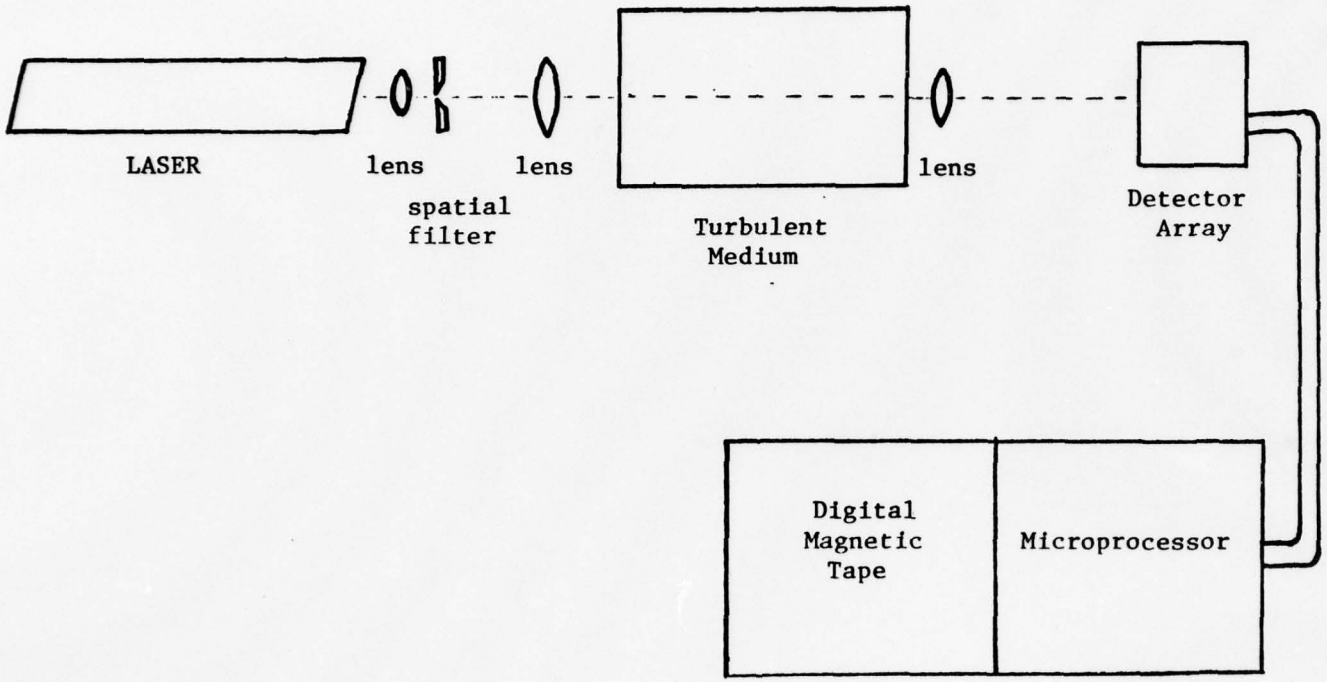

Figure 1

Schematic Illustration of
Turbulent Liquid Scattering Tank System

3 cm high and 10 cm apart run transversely and longitudinally across the bottom of the tank. Figure 2 is a photograph of the scattering apparatus.

The properties of the turbulent liquid which are important to optical propagation are the spatial spectrum and the structure function of the refractive index fluctuations. Since these fluctuations are due to temperature fluctuations and the rate of change of the refractive index with temperature, dn/dt, is a known property measurement of the spatial spectrum, $\phi_T(\kappa)$, and the structure function, $D_T(r) = \langle |T(\vec{r}_o + \vec{r}) - T(\vec{r}_o)|^2 \rangle$, of the temperature is sufficient.

Structure functions were determined by means of two 2.5 μm dia. 1.5 mm long platinum wire probes of nominal 40 Ω resistance, a Contel MT-2 microthermal analyzer, and the digital recording apparatus described above. The probe spacing was varied from 2 to 50 mm. The spatial spectra were recorded with a single probe (TSI Model 1276) consisting of a 25 μm diameter glass fiber plated with platinum. The length of the active region of the probe is 250 μm and it is presumed that it can resolve scale sizes of this order. The time response of the probe was measured to be ~ 10 ms. A reversible drive lead screw assembly controlled by the microprocessor was used to translate the probe through the liquid and the temperature recorded digitally. The bandwidth of this recording system (~ 100 Hz) exceeds by about an order of magnitude that of the temperature fluctuations which were observed in our experiments.

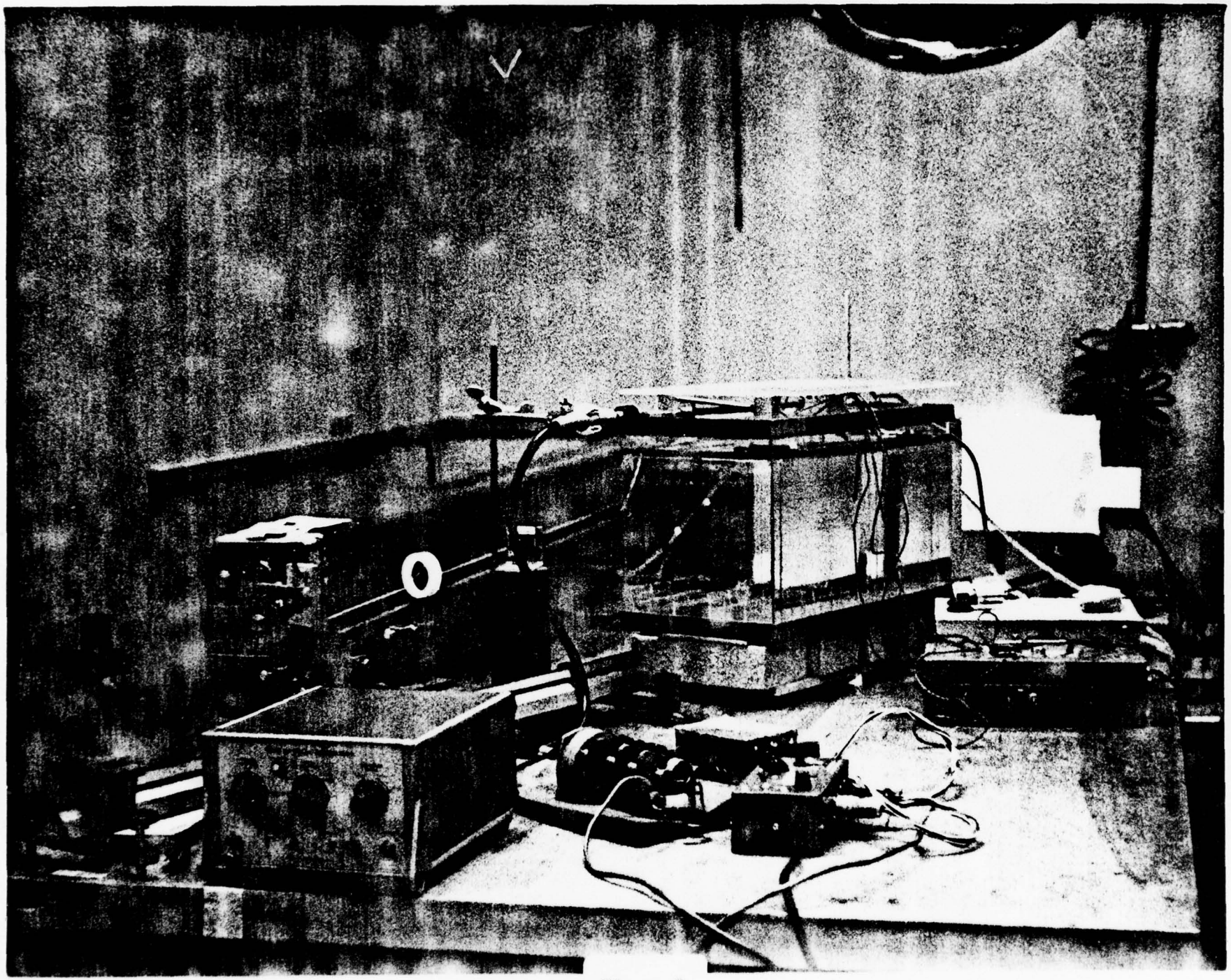

Figure 2

(iii) Experimental Results

a) Turbulence Measurements

The turbulent temperature fluctuations observed with this system exhibit virtually the same properties observed in atmospheric thermal turbulence. These include the 'spikey randomness' characteristic of small scale turbulence variables and both spatial and temporal intermittency often seen in the atmospheric variables. The only significant qualitative difference we have noted is the time scale of the fluctuations. In the atmosphere the bandwidth of the fluctuations determined by the small scale sizes of the order of millimeters and wind velocities of the order of meters/sec, is in the hundreds of hertz up to several kilohertz. In the tank, the small scale sizes of the fluctuations are also in the millimeter range but the characteristic velocities are centimeters/sec or less, thus yielding signal bandwidths of the order of 1 to 10 hertz. Figure 2 displays a single short trace of the thermal fluctuations observed with the platinum thin film probe. In this example, the probe was moving through the liquid at 1 cm/sec. The fluctuations observed are on the order of 0.1° and indicate scale sizes of significant energy in the range 1 mm - 1 cm.

Power spectra of the thermal fluctuations were obtained by fourier transforming recordings of the temperature like the one displayed in Fig. 3. Spatial spectra were inferred from these by dividing the frequency by the probe velocity (1 cm/sec) and multiplying by 2π. An example of such a spatial spectrum which

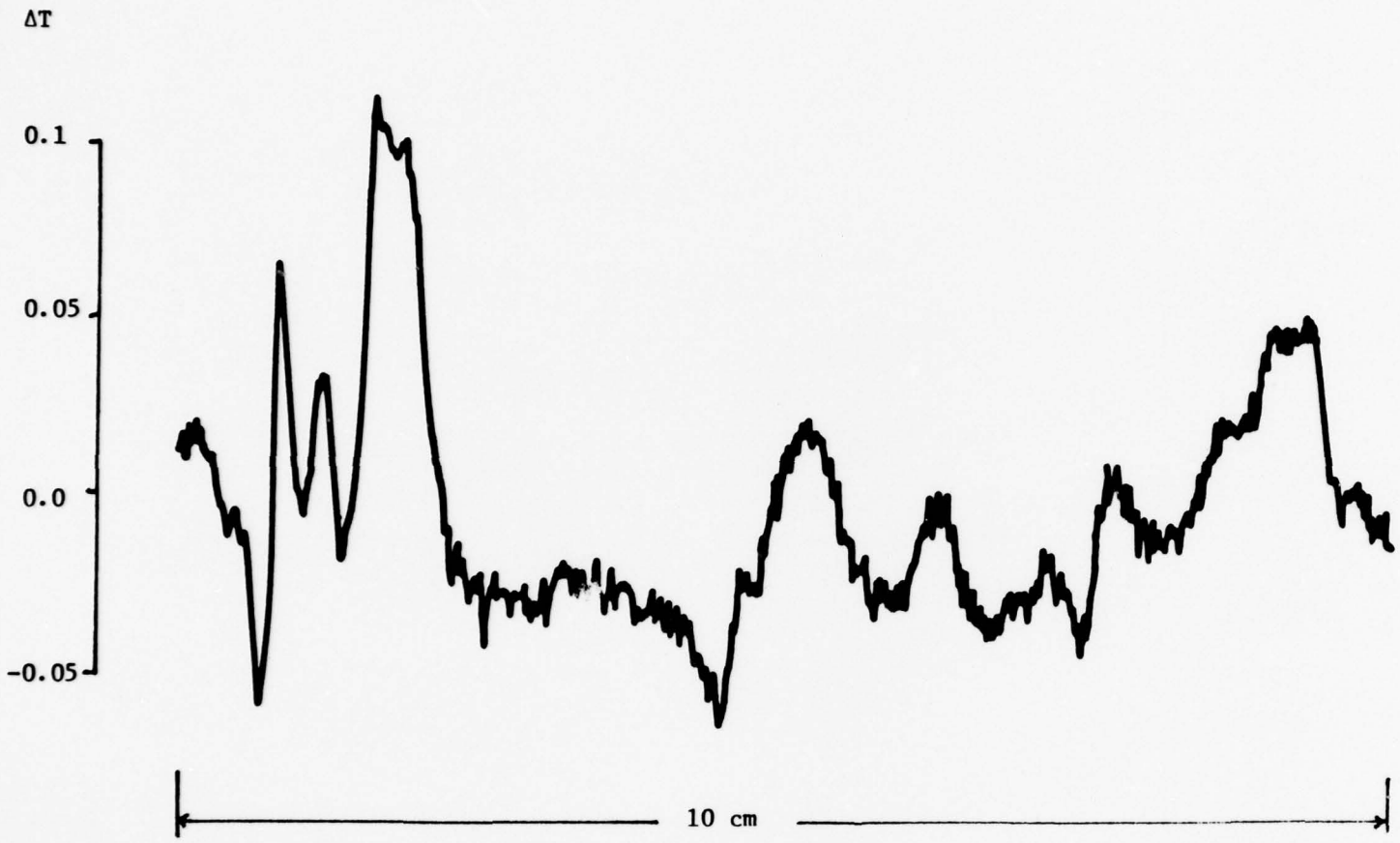

Figure 3

Temperature vs position. 250 μm × 25 μm dia. cylindrical thin film probe. Probe speed 1 cm/sec.

resulted from data obtained from 60 traverses of the probe is shown in Fig. 4. We note that the energy is down by four orders of magnitude for $k \gtrsim 100$ cm^{-1}, i.e., for scale sizes less than 0.6 mm.

Once a spectrum has been obtained by this method and stored in the computer it is a trivial matter to fit it to curves derived from the various theoretical models. As mentioned earlier Hill[10] and Hill and Clifford[12] have determined that one-dimensional spectra for high Reynolds number flows should have an inertial-convective range where it behaves as $\kappa^{-5/3}$, a viscous-convective range varying as κ^{-1} and a viscous-dissipative range which decays exponentially. Multiplying our experimentally determined spectra by $\kappa^{5/3}$ or κ^{-1} and replotting should therefore reveal flat portions corresponding to the inertial-convective or viscous-convective ranges respectively. Fig. 5 displays the spectrum of Fig. 4 multiplied by $\kappa^{5/3}$. It is evident that the small wave number portion of the data is not flat indicating that there is not a well defined inertial-convective range. The form of the one-dimensional spectrum expected at higher wave numbers in a system with a large Prandtl number is[12] $\phi_T(\kappa) = A\kappa^{-1} \exp(-\kappa\ell_1)$ where the scale ℓ_1 is related to the Kolmogorov microscale η by $\eta = \ell_1 p_r^{1/2}/5.5$. The best least squares fit of this curve to the data used in Figs. 4 and 5 is shown in Fig. 6. Fig. 7 displays a strictly empirical fit of the same data to $\phi_T(\kappa) = B(\kappa + 2\kappa^3)^{-1}$, and Fig.8 shows the best fit provided $\phi_T(\kappa) = c\kappa^{-1} \exp(-\alpha\eta^2\kappa^2)$, the Batchelor spectrum assumed by Gurvich et al.[14]

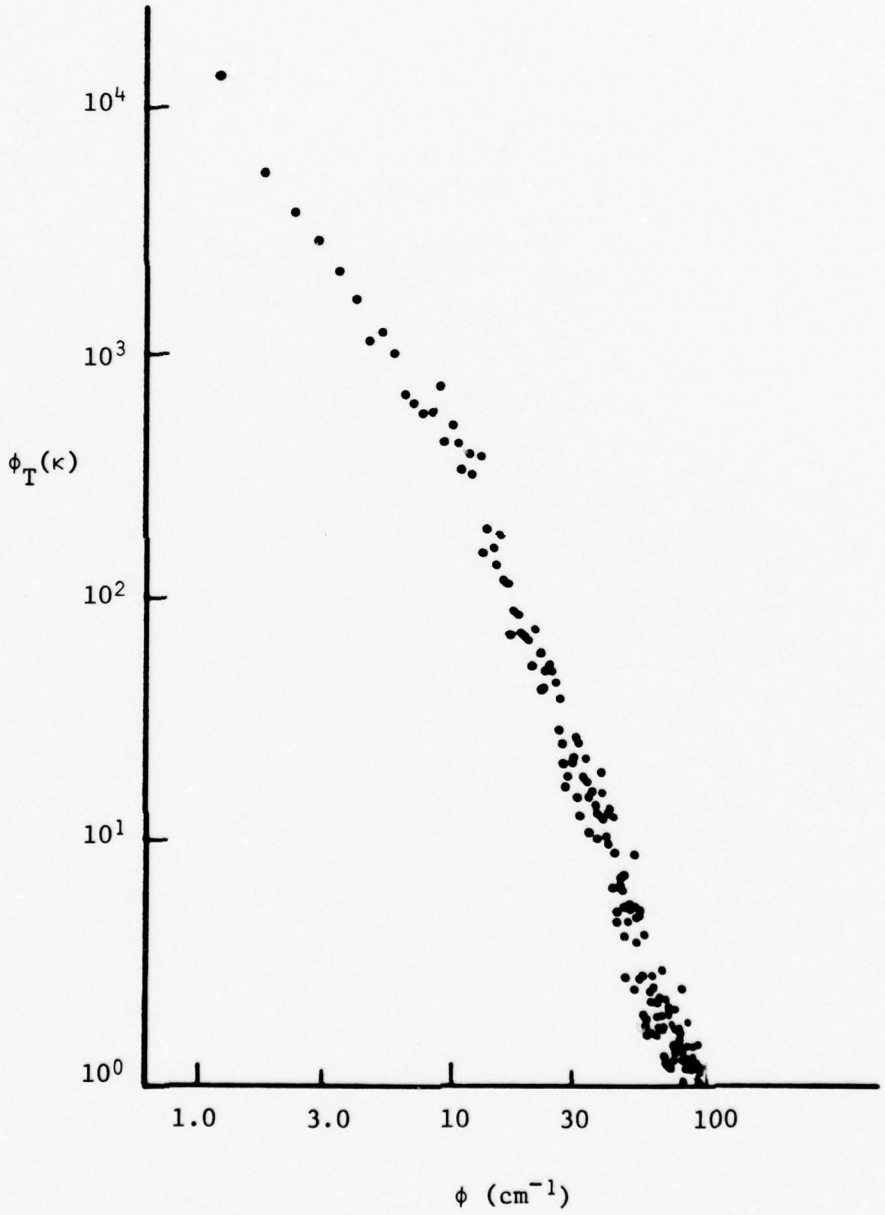

Figure 4 Spatial spectrum of temperature fluctuations

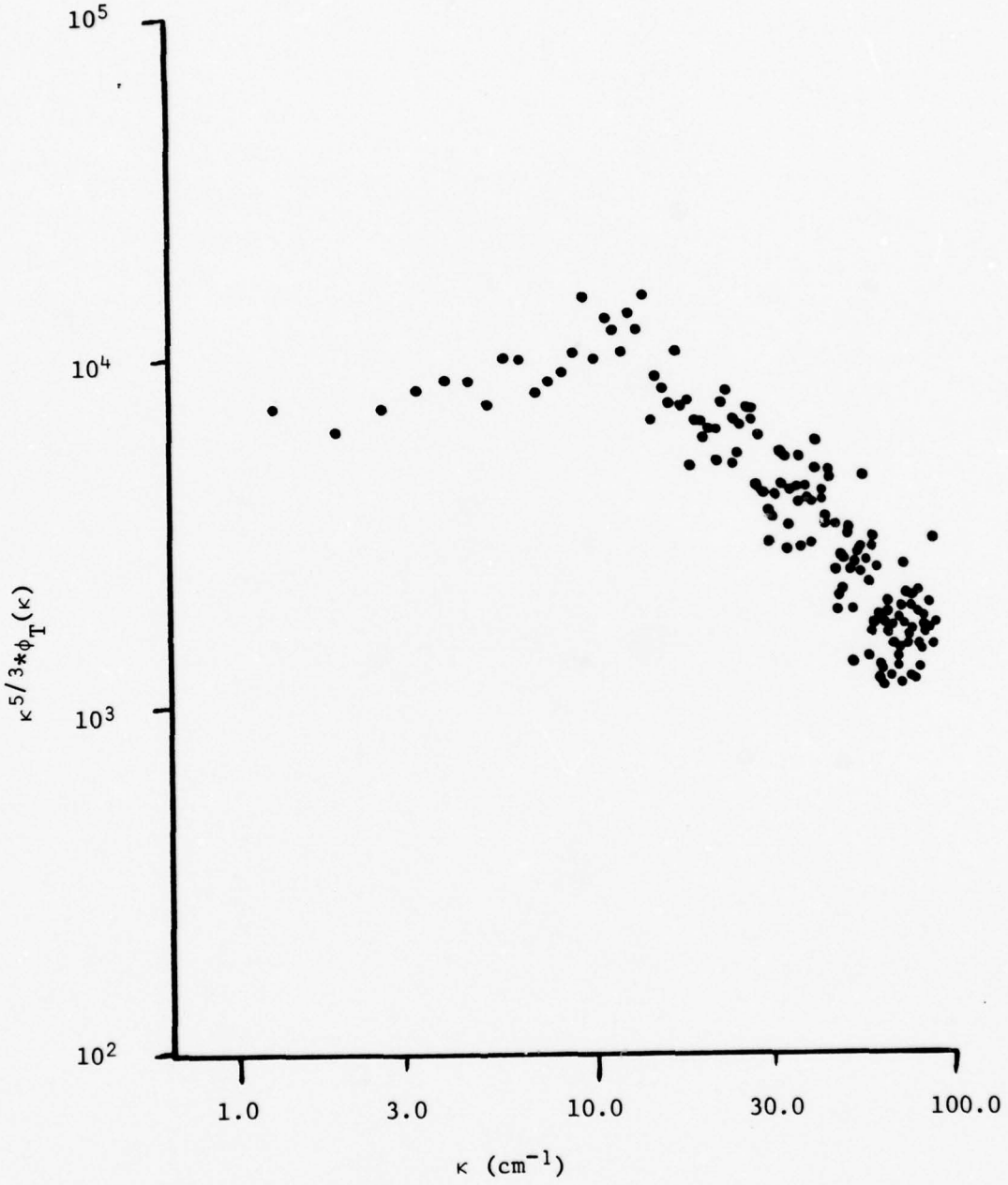

Figure 5 Experimental Spatial Spectrum Multiplied by $\kappa^{5/3}$

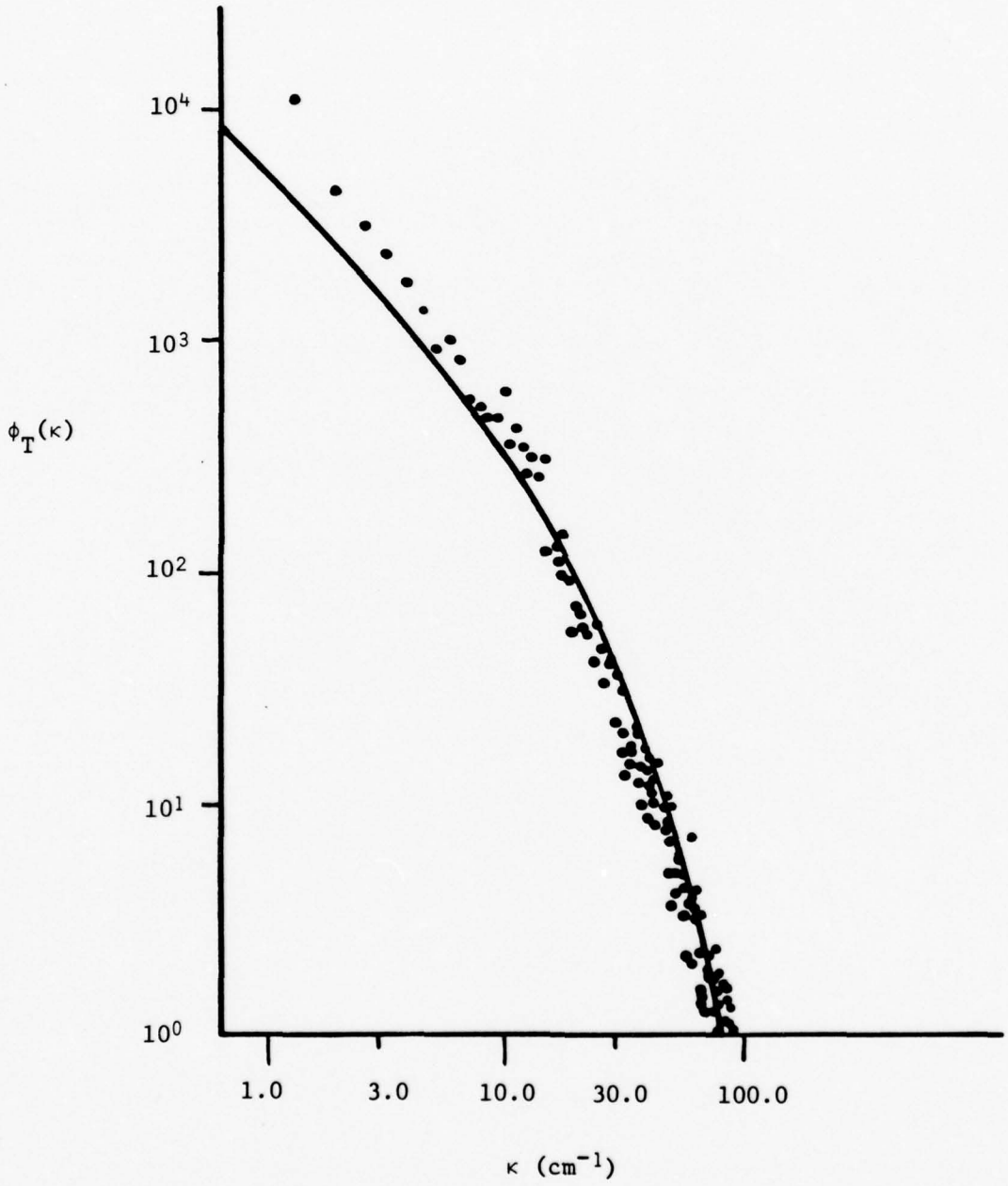

Figure 6 Spatial Power Spectrum of Temperature Fluctuations.
Solid Line - Hill Spectrum (one dimension)

$$\phi_T(\kappa) = \frac{A}{\kappa} \exp(-\kappa \ell_1) \text{ where } \ell_1 = 0.055 \text{ cm}$$

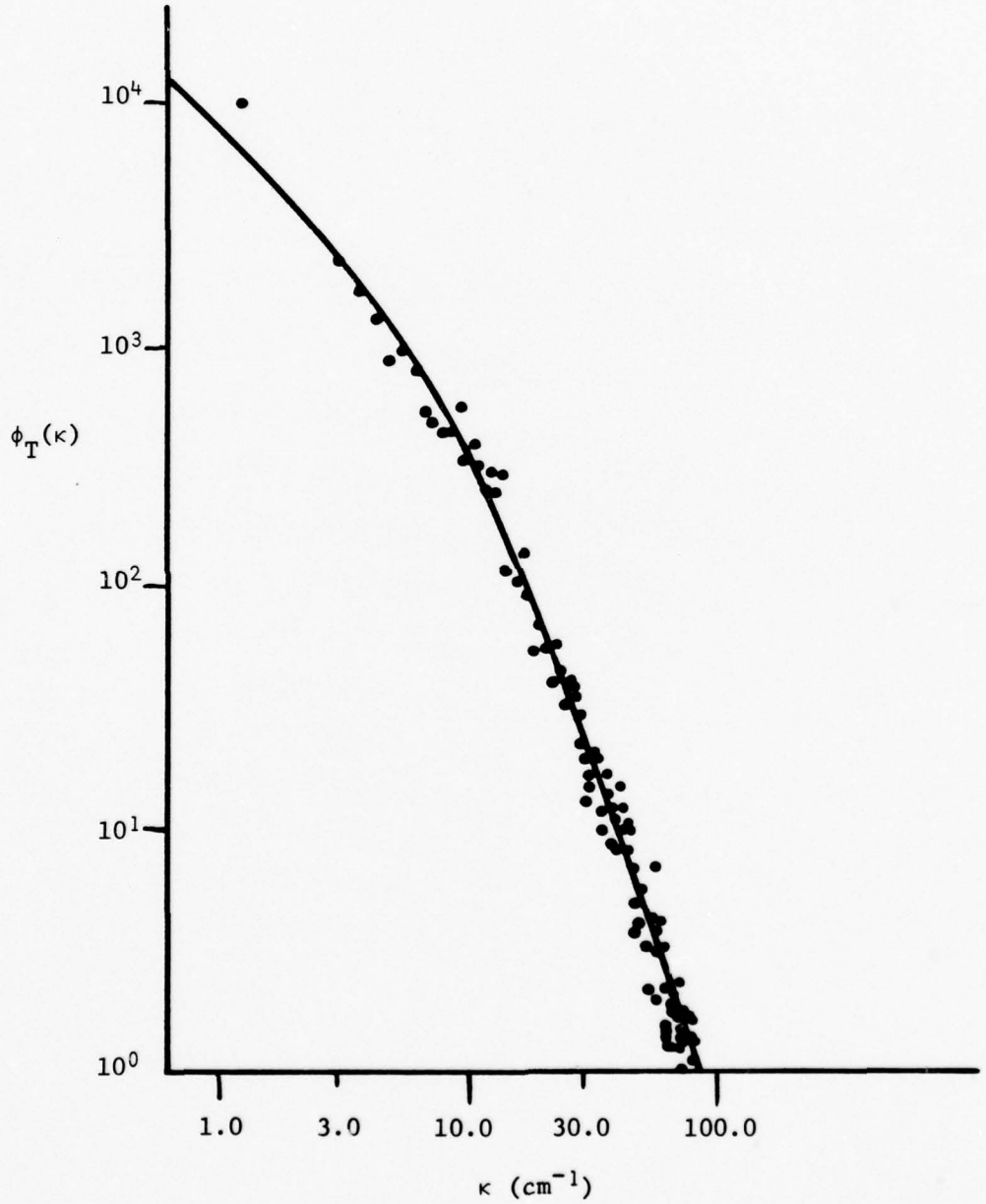

Figure 7 Spatial power spectrum of temperature fluctuations.

Solid line is $\phi_T(\kappa) = \frac{B}{\kappa + b^2\kappa^3}$ where b = .114 cm.

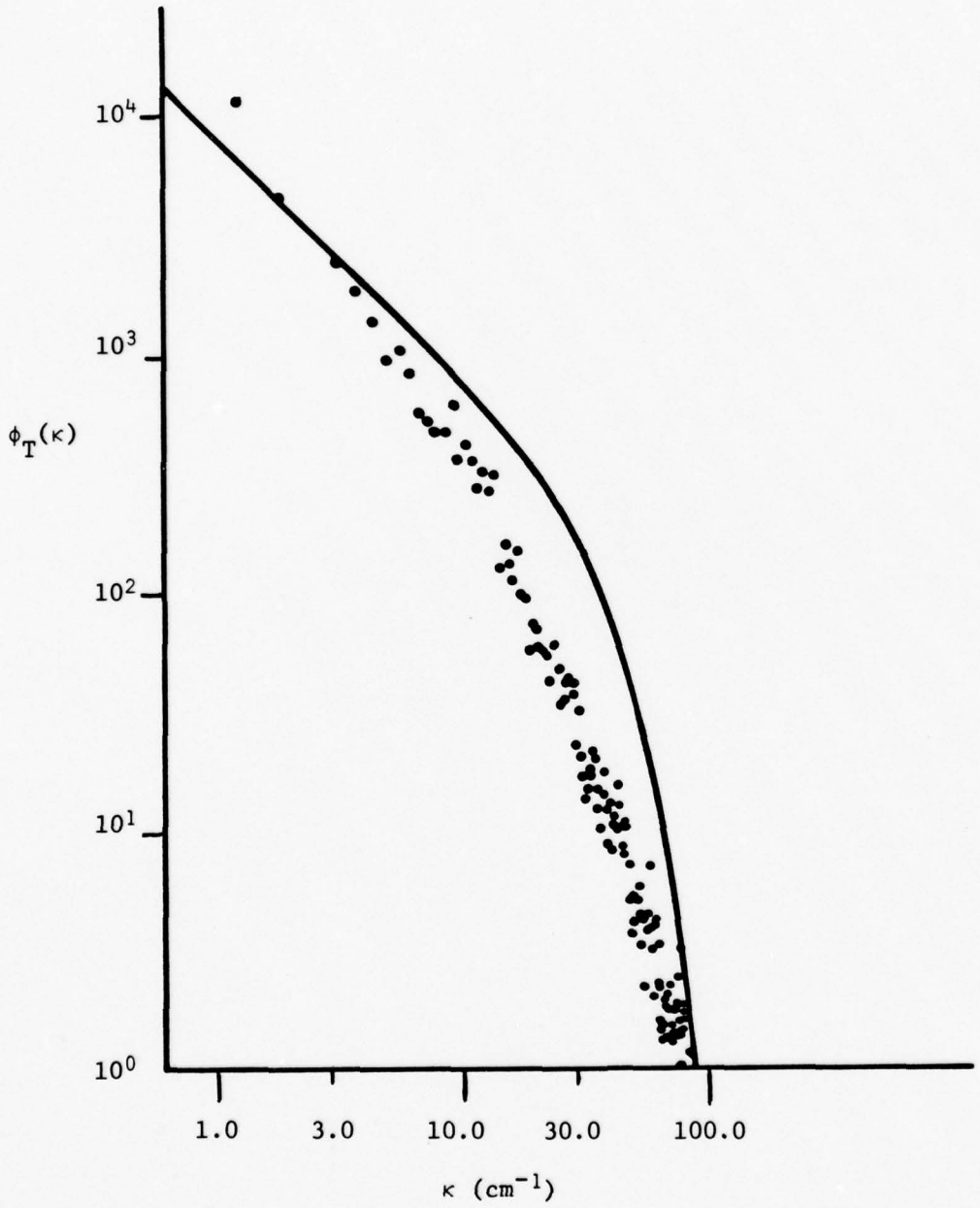

Figure 8 Spatial power spectrum of temperature flucuations.

Solid line - Batchelor Spectrum $\phi_B(\kappa) = \frac{C}{\kappa} \exp(-\alpha\kappa^2\eta^2)$

where $\eta\sqrt{\alpha} = .025$ cm.

The empirical fit to $B(\kappa + b^2\kappa^3)^{-1}$ clearly agrees best with the experimental data, a point made more dramatically evident in Figs. 9, 10, and 11 where the data points have been multiplied by κ^{-1} $\exp(-\kappa\ell_1)$, $(\kappa + 2\kappa^3)^{-1}$, and $\kappa^{-1}\exp(-\alpha\kappa^2)$ respectively and replotted. The points should lie on a horizontal line.

We may compare the value of η determined by the value of ℓ_1 required to fit the Hill spectrum to the experimental spectrum with that calculated on the basis of the physical parameters of the fluid and the amount of power put into the tank. The Kolmogorov microscale is given by

$$\eta = \left(\frac{\nu^3}{\epsilon}\right)^{1/4}$$

where ν is the viscosity and ϵ the energy dissipation rate. The dissipation rate[14]

$$\epsilon \approx \frac{g\, B_T q_T}{C_p\, \rho}$$

where g is the gravitation acceleration, B_T the coefficient of thermal expansion, q_T the turbulent heat flow related to the heating power applied to the tank, C_p the specific heat and ρ the density. For an input power of 900 watts, tank area 1250 cm^2, and the parameter values appropriate to ethanol given in Table I we have $\epsilon = 0.09\ cm^2/sec^3$. This in turn yields a length scale of $\eta = 0.054$ cm. This agrees quite well with the experimentally determined value of $\eta = \ell_1 p_r^{1/2}/5.5 = 0.04$ cm. It is noteworthy that the length scale characteristic of the spectrum depends on

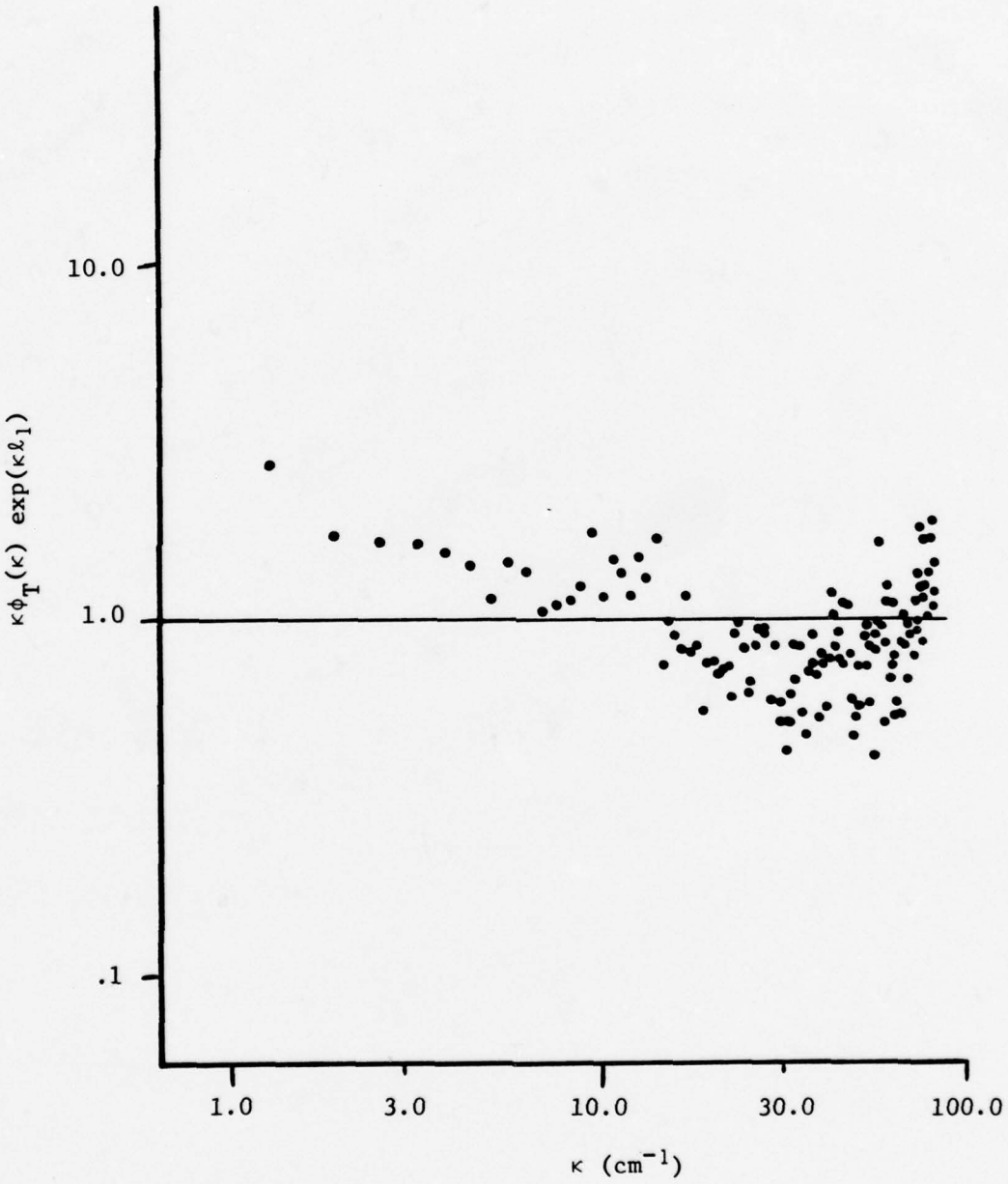

Figure 9 Ratio of experimental spatial spectrum to Hill spectrum

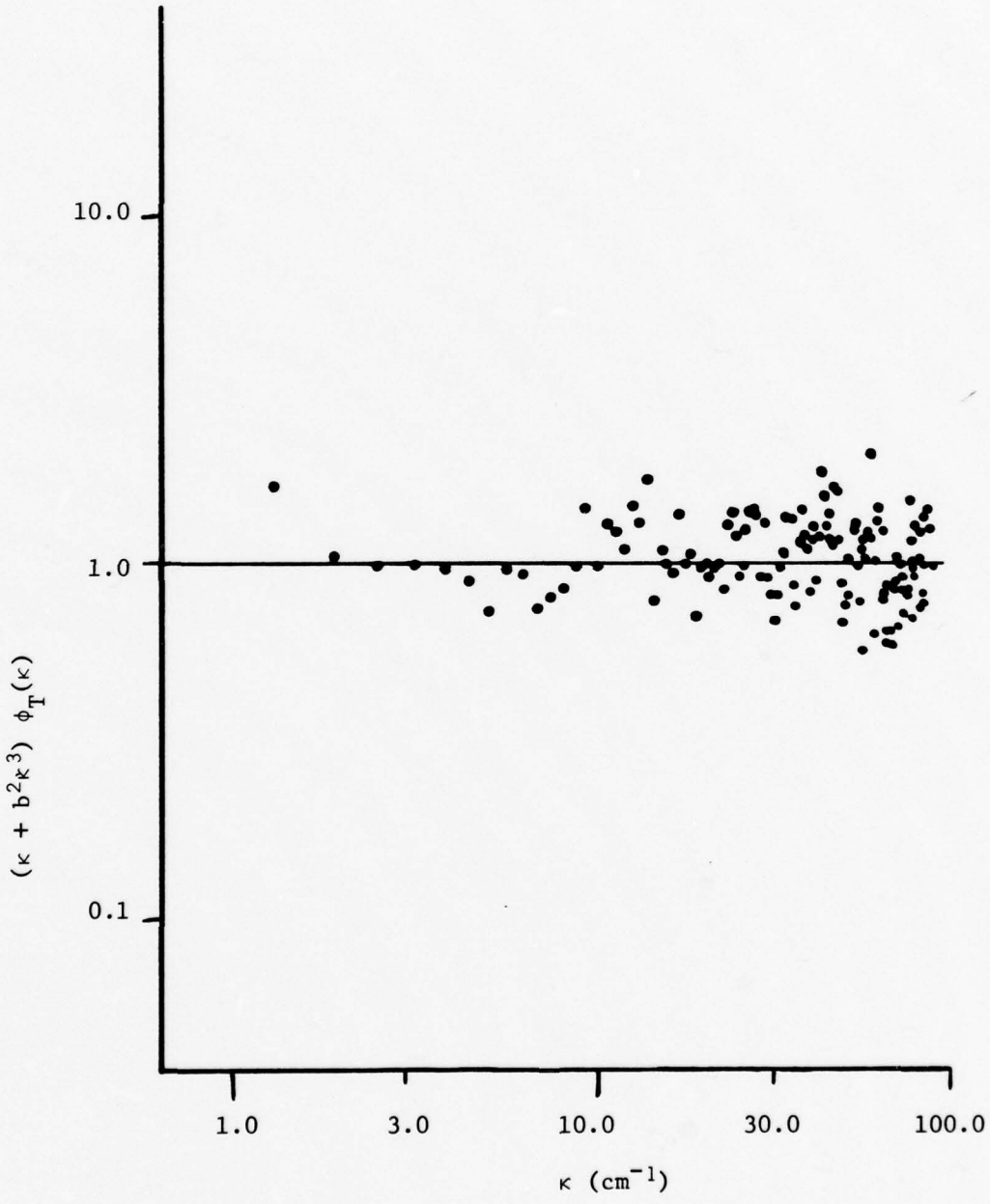

Figure 10 Ratio of experimental spatial spectrum to

$$\phi_T(\kappa) = \frac{1}{\kappa + b^2\kappa^3}$$

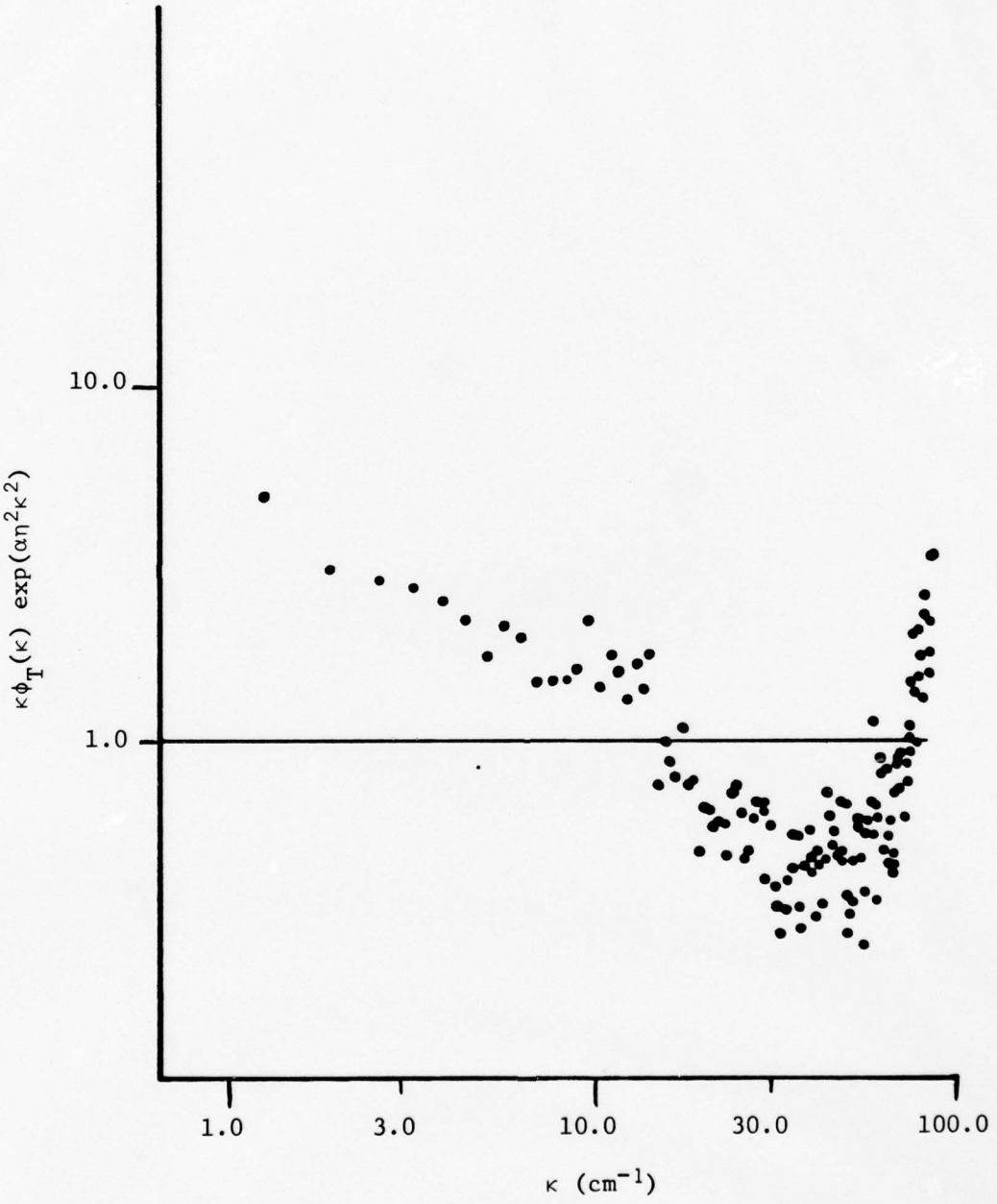

Figure 11 Ratio of experimental spatial spectrum to Batchelor Spectrum

Table I

Properties of Ethanol

density	ρ	0.79 gm/cm^3
index of refraction	n	1.361
	dn/dT	-4×10^{-4}/°C
viscosity	ν	1.5×10^{-2} cm^2/sec
coefficient of thermal diffusivity	D	$\sim 9.4 \times 10^{-4}$
coefficient of thermal expansion	B_T	0.0011/°C
specific heat	C_p	.574 cal/gm°C
Prandtl No.	P_r	16

$\epsilon^{-1/4}$. Thus, all other parameters and conditions being equal, the position of the spectrum of the thermal fluctuations is very insensitive to the power in the turbulence; for example, a 10-fold increase in heat flow q_T yields a 10-fold increase in the dissipation rate ϵ, but only an increase of the order of 1.75 in the value of ℓ_1. Thus although the characteristic length scales η and ℓ_1 vary with the power input, the variation is weak enough that a single value of ℓ_1 is applicable to a substantial range of heater power levels.

At this time it may be noted that Bissonette[13] reported observations indicating that a -5/3 slope inertial-convective range

spectrum did obtain in his experiments in turbulent water. However his spectra were determined with a stationary probe. We show in Fig. 12 an example of a power spectrum derived from stationary probe recordings of the thermal fluctuations in our ethanol tank. This data multiplied by $f^{5/3}$ is replotted in Fig. 13 and clearly exhibits a flat portion at the low frequency end. We infer from this that the -5/3 slope is an artifact of measuring the spectra with a stationary probe.

The spatial spectrum of index of refraction fluctuation is just the spectrum of temperature fluctuations multiplied by $(dn/dT)^2$, in this case 1.6×10^{-7} °C^{-2}. Although all the information about the turbulent field that is relevant to optical propagation is contained in this function propagation theories are often couched in terms of the structure function which may be calculated from the 3-dimensional spectrum, $\psi_n(\kappa) = -\frac{1}{2\pi\kappa}\frac{d\phi_n(\kappa)}{d\kappa}$, by

$$D_n(r) = 8\pi \int_0^\infty \left(1 - \frac{\sin \kappa r}{\kappa r}\right) \psi_n(\kappa)\, \kappa^2\, d\kappa \qquad (1)$$

We use the Hill spectrum, $\phi_n(\kappa) = A' \kappa^{-1} \exp(-\kappa \ell_1)$ with $A' = (dn/dT)^2 A$ and $\ell_1 = 0.55$ mm as determined above, since it leads to a simple analytic result and since it has some theoretical justification. The 3-D spectrum is in this case $\psi_n(\kappa) = \frac{A'}{2\pi} \kappa^{-3} (1 + \kappa\ell_1) \exp(-\kappa\ell_1)$ and

$$D_n(r) = \tilde{C}_n^2\, \ell n(1 + (r/\ell_1)^2) \qquad (2)$$

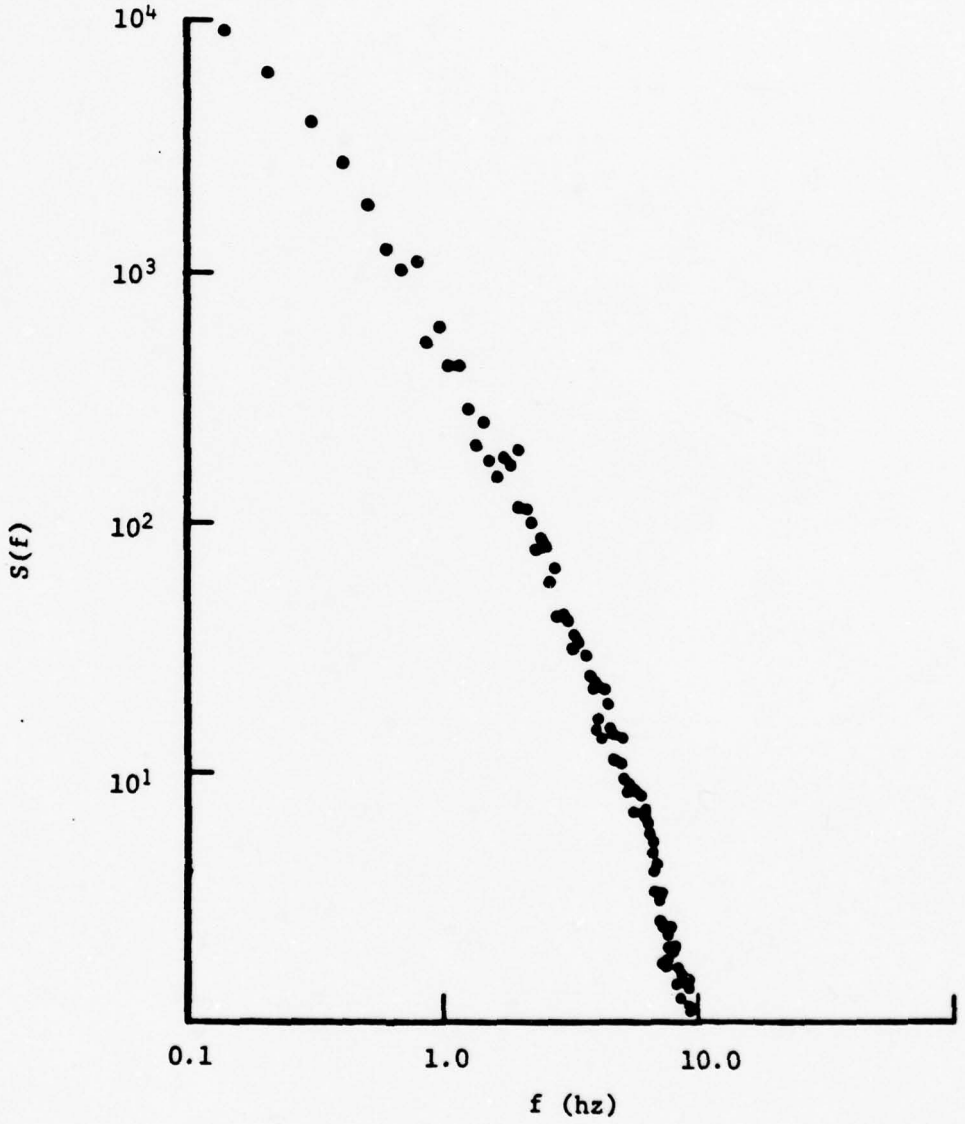

Figure 12

Power spectrum of temperature fluctuations. 250 μm × 25 μm dia. cylindrical thin film probe. Probe stationary.

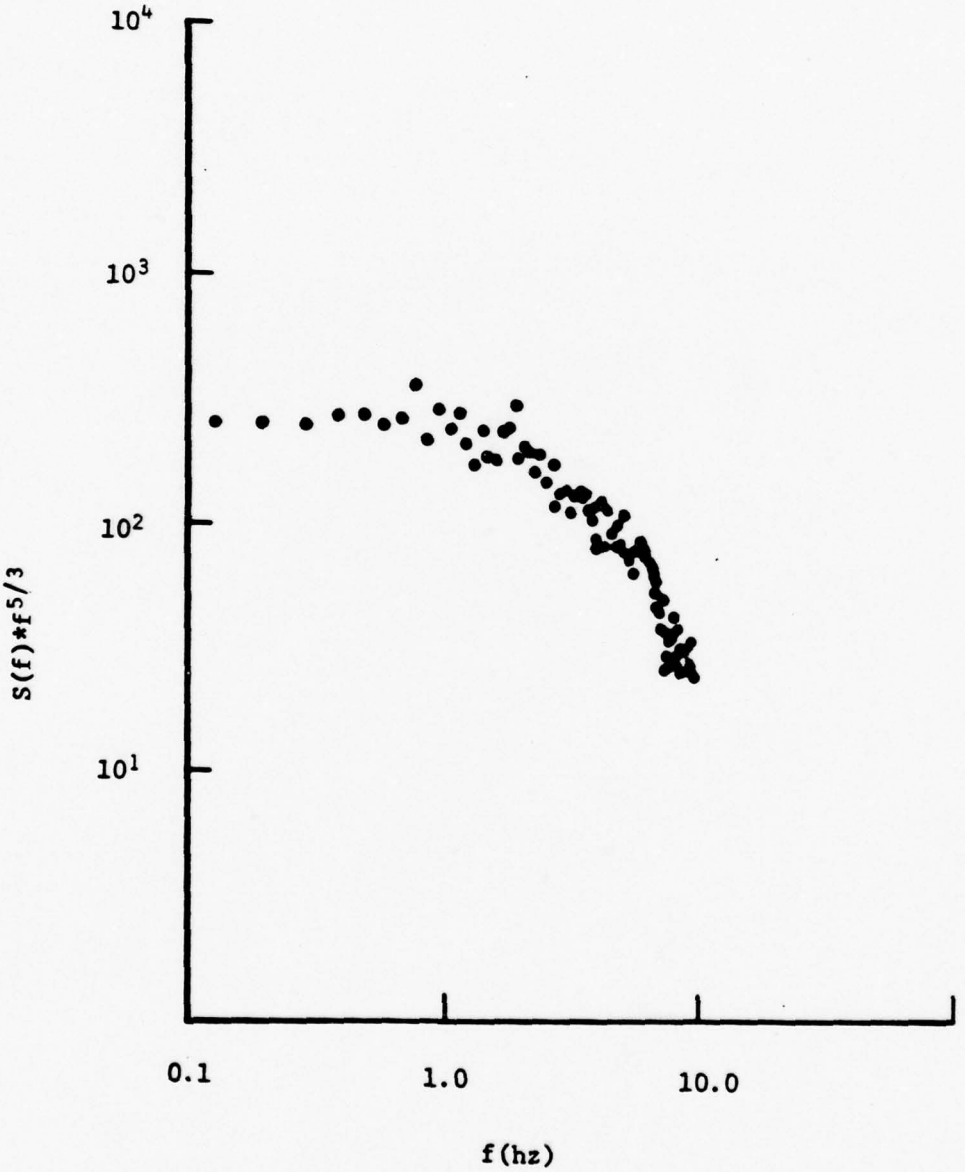

Figure 13

Power spectrum of temperaure fluctuations multiplied by $f^{5/3}$.

where $\tilde{C}_n^2 = 2A'$ is a parameter describing the strength of the index of refraction fluctuations and corresponds to the usual structure parameter C_n^2. Fig. 14 shows a plot of this structure function together with values of $\langle |n(\vec{r}_o + \vec{r}) - n(\vec{r}_o)|^2 \rangle$ obtained from half-hour averages of the square of the temperature difference. This exhibits nice agreement over the central portion of the curve. The deviation at small separations can be explained by the inability of our 1.5 mm long probes to adequately resolve scale sizes of this magnitude.

The strength of the turbulence can be characterized by the constant $\tilde{C}_n^2$ and this is readily measured by determining $D_n(r)$ for some convenient value of r. Fig. 15 is a plot of $\tilde{C}_n^2$ determined in this way, with r = 1 cm, as a function of heater power. The values of $\tilde{C}_n^2$ range over nearly two orders of magnitude from 5×10^{-11} to 2×10^{-9}.

b) Optical Propagation

In part a) above we have described the characteristics of the turbulence in our simulation apparatus and have noted that the spatial spectrum of the temperature or index of refraction fluctuations is different from that observed in the atmosphere. The optical path length in our system is also much shorter than typical atmospheric propagation paths. The scale sizes of the turbulent eddies is somewhat different from those in the atmosphere and since the Fresnel zone size in our system is much smaller than would be

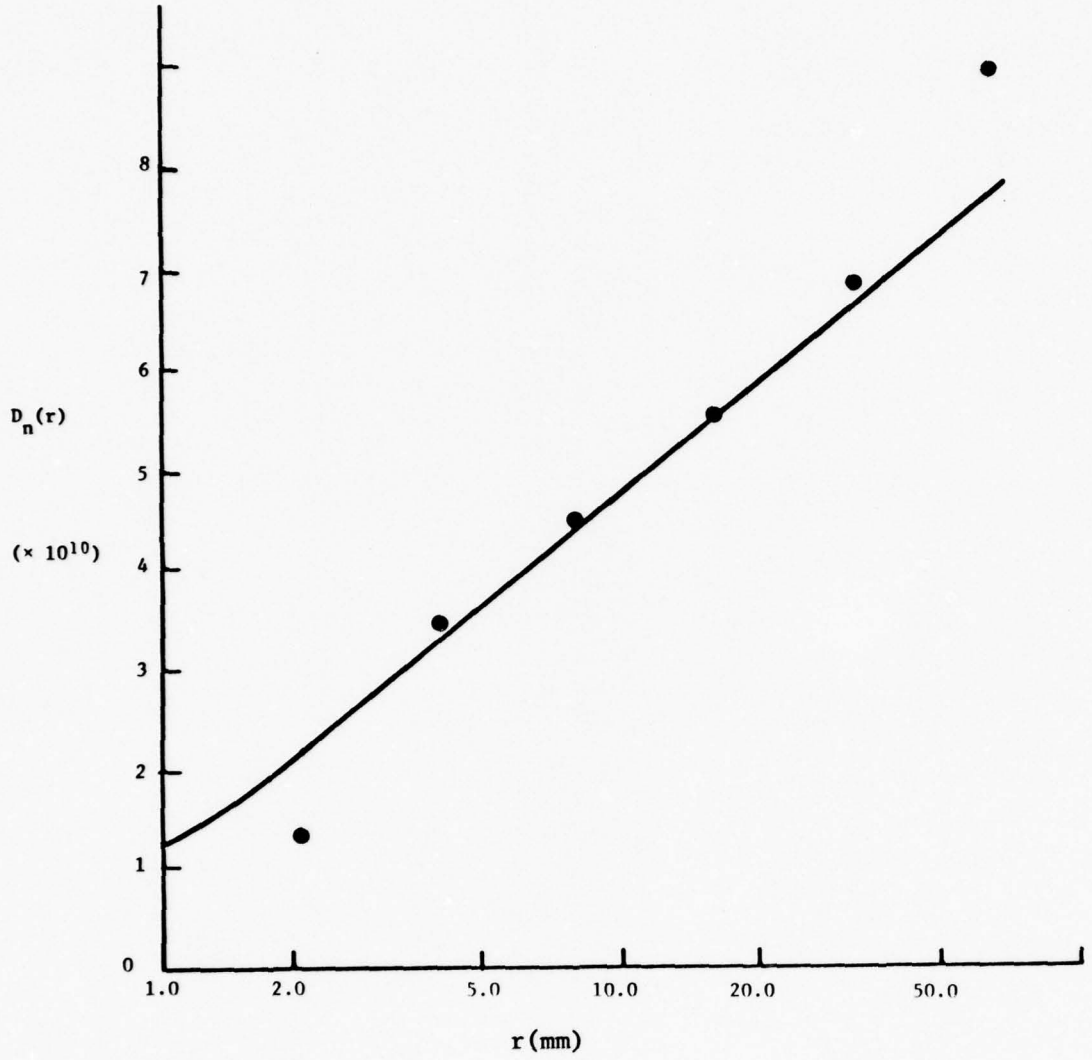

Figure 14 Structure function of index of refraction fluctuations

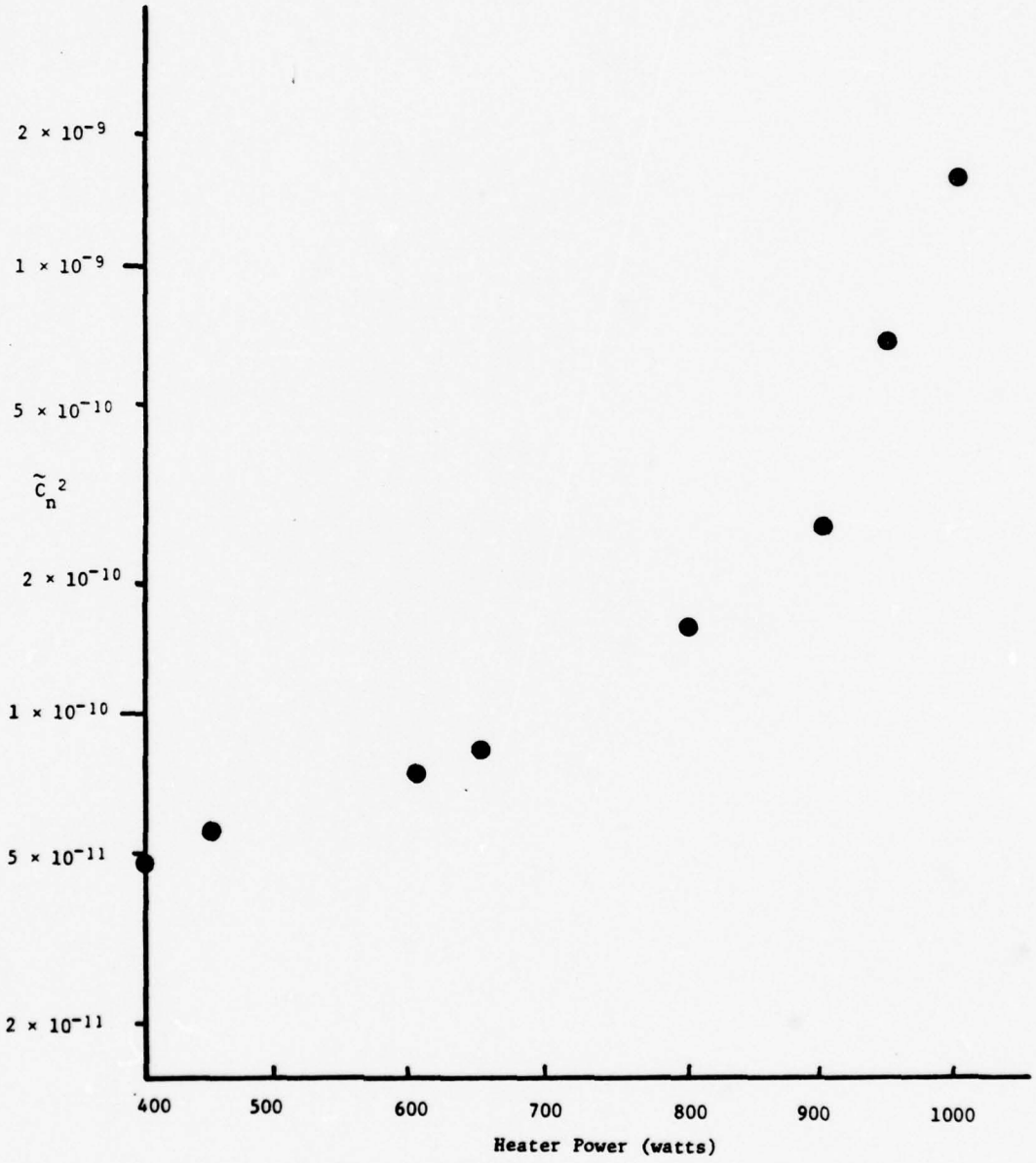

Figure 15 Turbulent intensity level $\tilde{C}_n^2$ versus applied heater power.

the case for a field experiment ($\sqrt{\lambda L}$ = 0.48, 0.83 or 1.08 mm depending on whether 1, 3 or 5 passes are made through the tank) the important eddy sizes are also significantly smaller. We therefore expect that some features of the radiation field may differ from those observed over long atmospheric paths. In particular we anticipate a smaller bandwidth for the intensity fluctuations due to the slower variation in index of refraction fluctuations. Also the scintillation patch size should be smaller and aperture averaging effects may be important if the detector size is not sufficiently small.

Records of the irradiance recorded at a single detector for the weakest and strongest path integrated turbulence are shown in Figs. 16 and 17. The values of $\sigma^2_{\ell nI}$ listed on the figures are the log-irradiance variance calculated in the Rytov approximation,[2] i.e.,

$$\sigma^2_{\ell nI} = 8\pi^2 k^2 L \int_0^\infty \left(1 - \frac{k}{\kappa^2 L} \sin \frac{\kappa^2 L}{k}\right) \psi_n(\kappa) \kappa \, d\kappa$$

with κ being the optical wave number, k the index of refraction wave number, L the path length and $\psi_n(\kappa) = \frac{\tilde{C}_n^2}{4\pi\kappa^3} (1 + \kappa\ell_1) \exp(-\kappa\ell_1)$ with ℓ_1 = 0.55 mm. These traces are qualitatively similar to the irradiance fluctuations observed in the atmosphere although in these laboratory results the time scale of the fluctuations is significantly slower.

The least well resolved of the basic questions concerning the statistical properties of theoretical field is the form of the

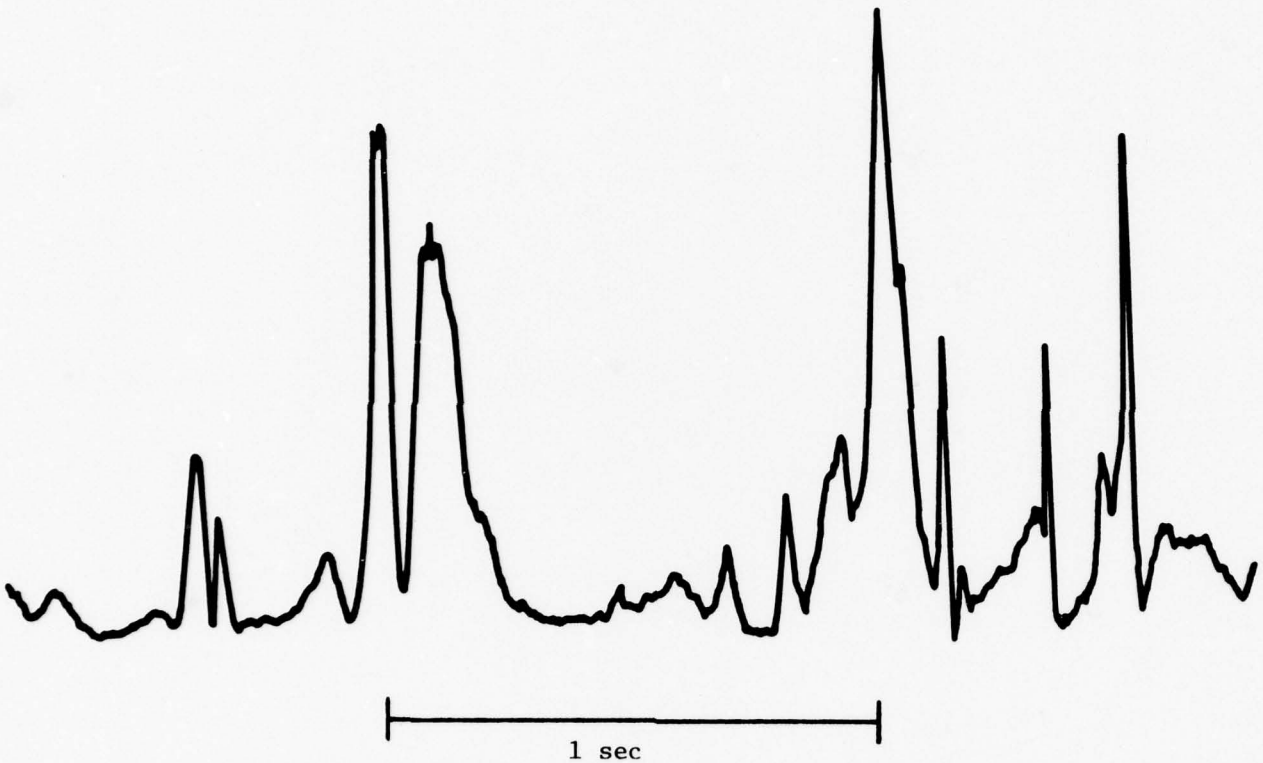

Figure 16

Point detector recording of irradiance. $\sigma^2_{\ell nI} = 0.11$

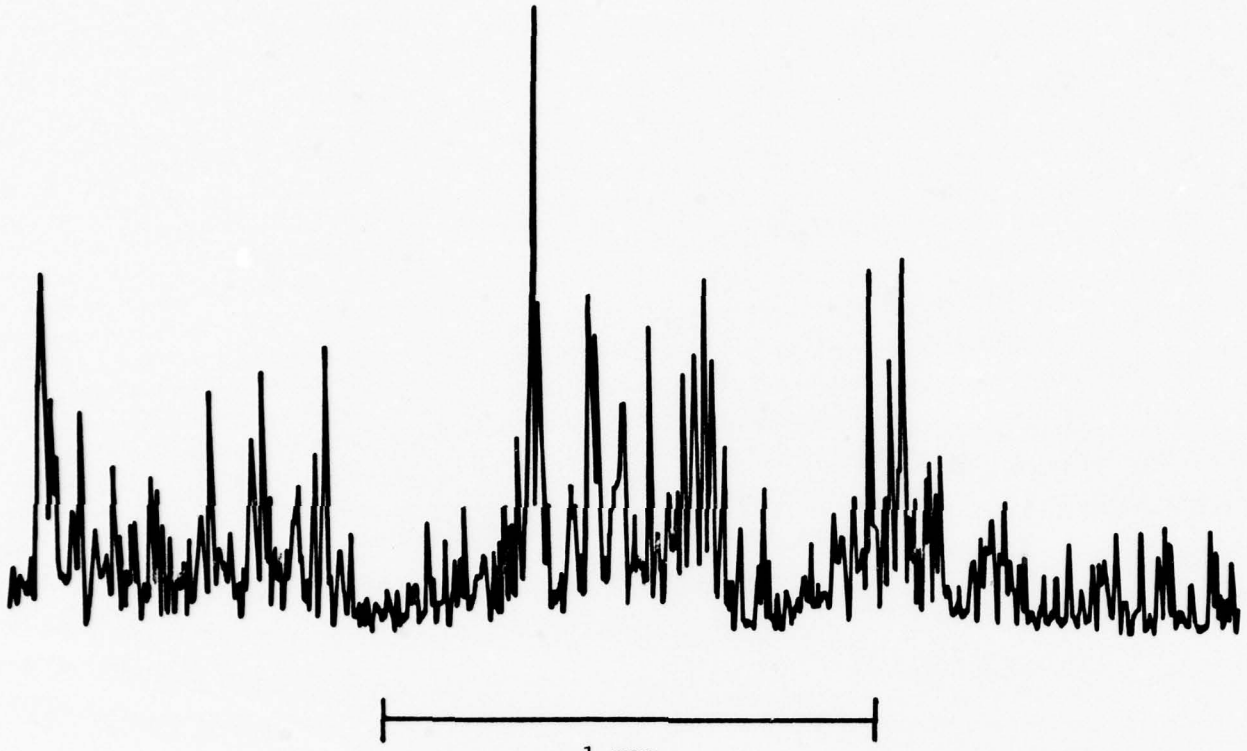

Figure 17 Point detector recording of irradiance. $\sigma^2_{\ell nI} = 210$

probability density function of the irradiance. It is generally accepted that the PDF of the irradiance is log normal in weak turbulence and exponential in an asymptotic state of very strong path integrated turbulence. Figures 18, 19, and 20 show the PDF of the irradiance in progressively stronger path integrated turbulence conditions. Also displayed in each figure are the maximum likelihood fits to the log normal and exponential functions. In each case the exponential function is a straight line. Fig. 18 is a weak turbulence short path condition and the distribution shows reasonable but imperfect agreement with the log normal assumption. Fig. 19 is a stronger turbulence condition. Here the normalized variance of the irradiance is near its peak, $\sigma^2_{I_N} = 2.86$, and while there is scatter in the data, the log normal distribution still yields a qualitatively good fit to the data. Finally Fig. 20 shows the distribution in the case of the strongest turbulence conditions observed in the system. In this case the data scatter encompasses both the exponential and log normal distributions except at very low irradiance values, and we cannot visually make a distinction. We have not been able to reach strong enough turbulence levels to unambiguously observe an exponential distribution. We note, however, that in this final example the normalized variance of the irradiance is 1.09, very close to the value of unity associated with the exponential distribution.

Fig. 21 is a plot of the normalized irradiance variance $\sigma^2_{I_N} = \sigma^2_I/\overline{I}^2$ as a function of turbulence level described by the

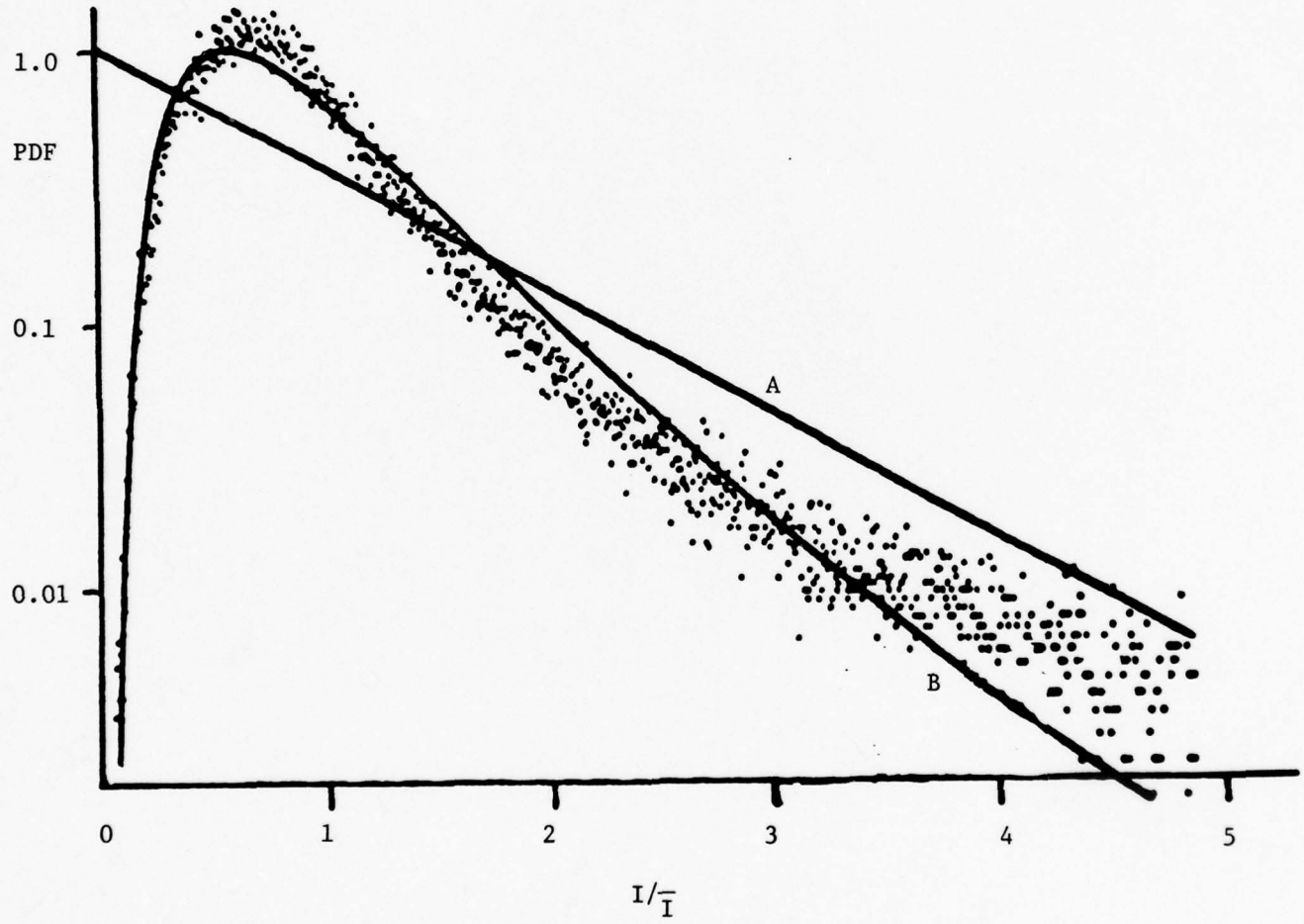

Figure 18 Probability density function of irradiance. L = 0.5m, Rytov $\sigma^2_{\ell nI}$ = 0.19. Experimental $\sigma^2_{I_N}$ = 0.72, $\sigma^2_{\ell nI}$ = 0.193.
A - maximum likelihood fit to exponential distribution
B - maximum lielihood fit to log-normal distribution

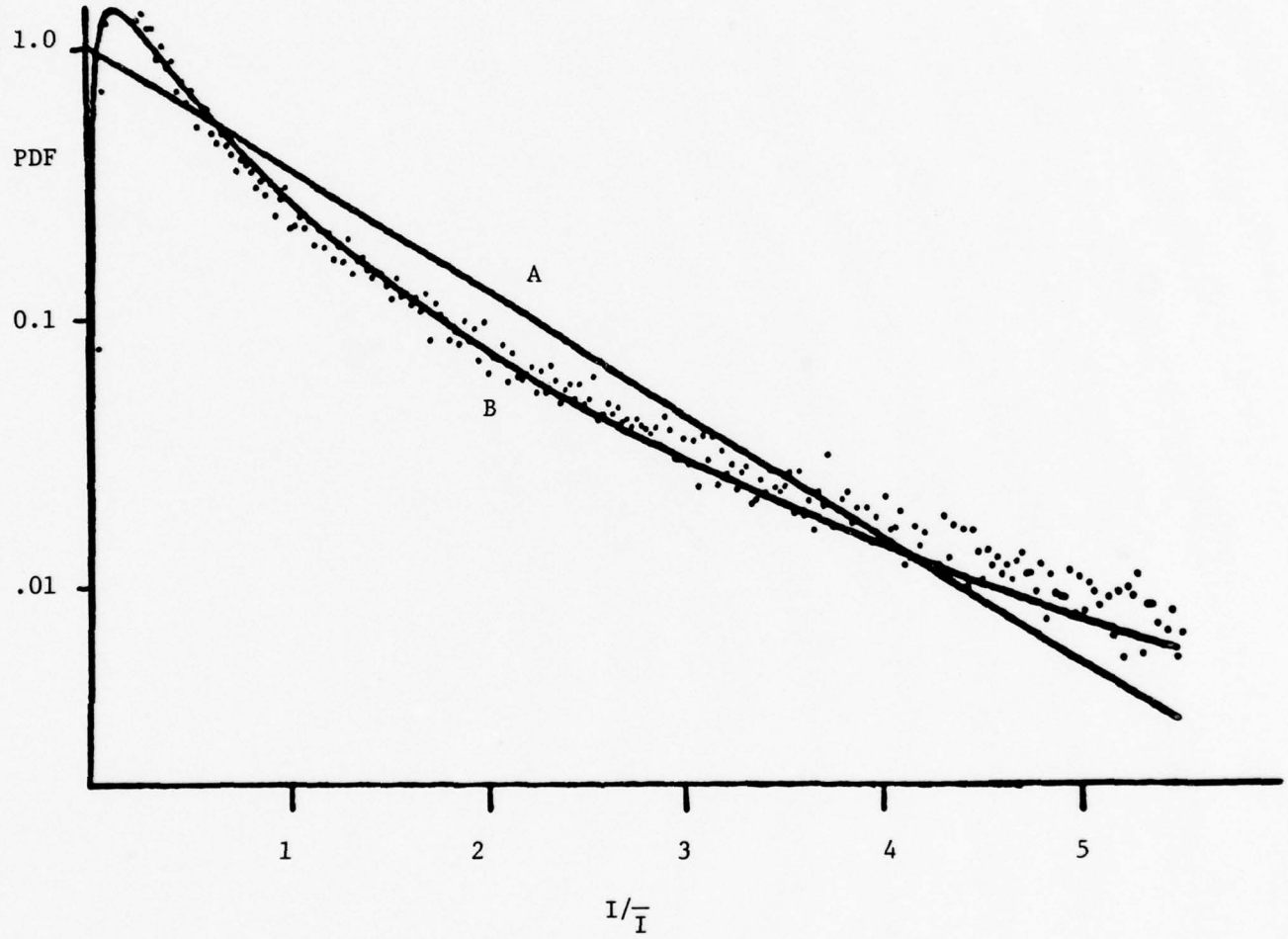

Figure 19 Probability density function of irradiance. L = 1.5 m, Rytov $\sigma^2_{\ell}nI = 3.5$. Experimental $\sigma^2_{I_N} = 2.86$, $\sigma^2_{\ell nI} = 1.32$.

A - maximum likelihood fit to exponential

B - maximum likelihood fit to log-normal

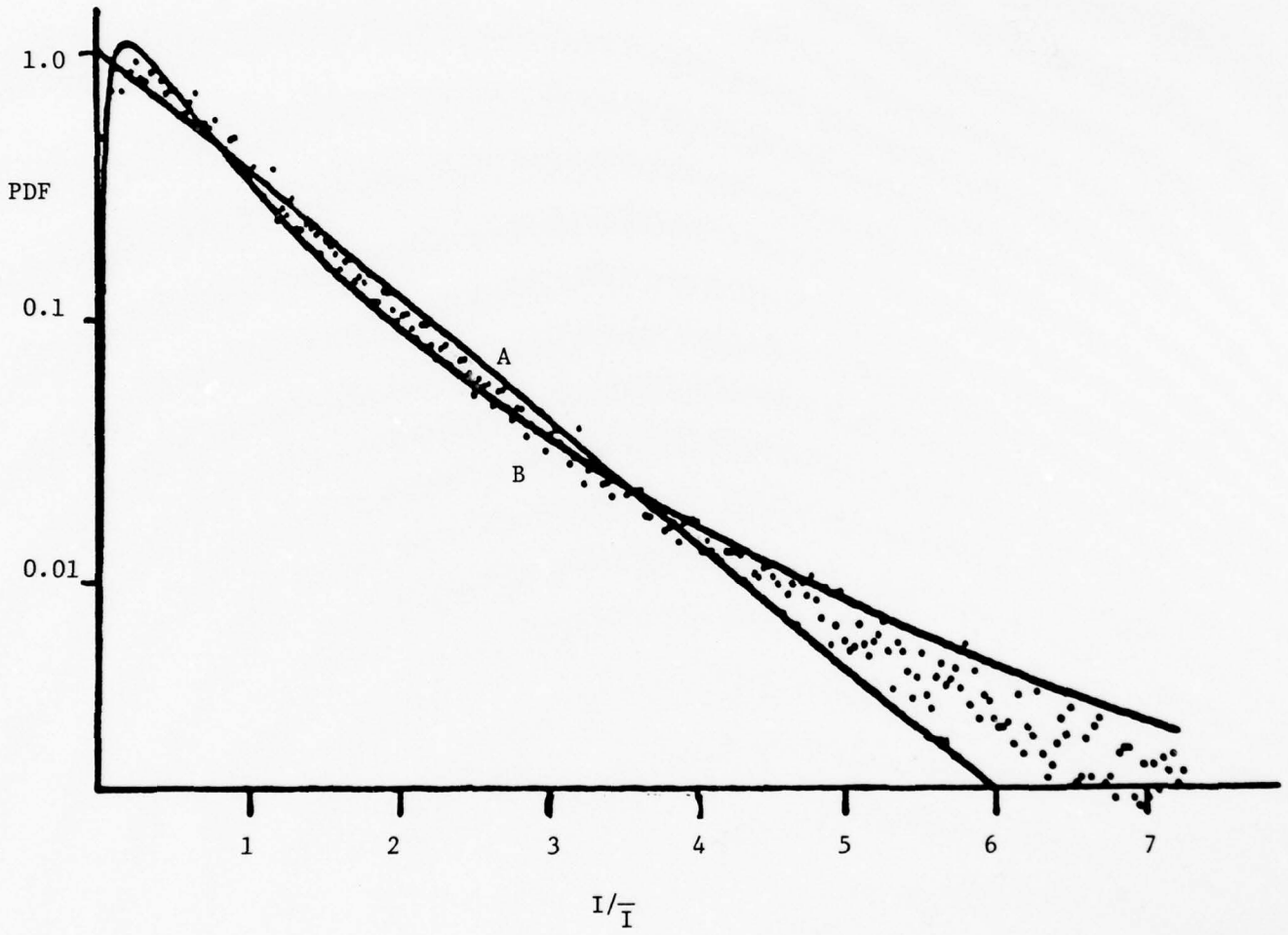

Figure 20 Probability density function of irradiance. L = 2.5 m, Rytov $\sigma^2_{\ell nI}$ = 210. Experimental $\sigma^2_{I_N}$ = 1.09, $\sigma^2_{\ell nI}$ = 0.766.

A - maximum likelihood fit to exponential

B - maximum likelihood fit to log-normal

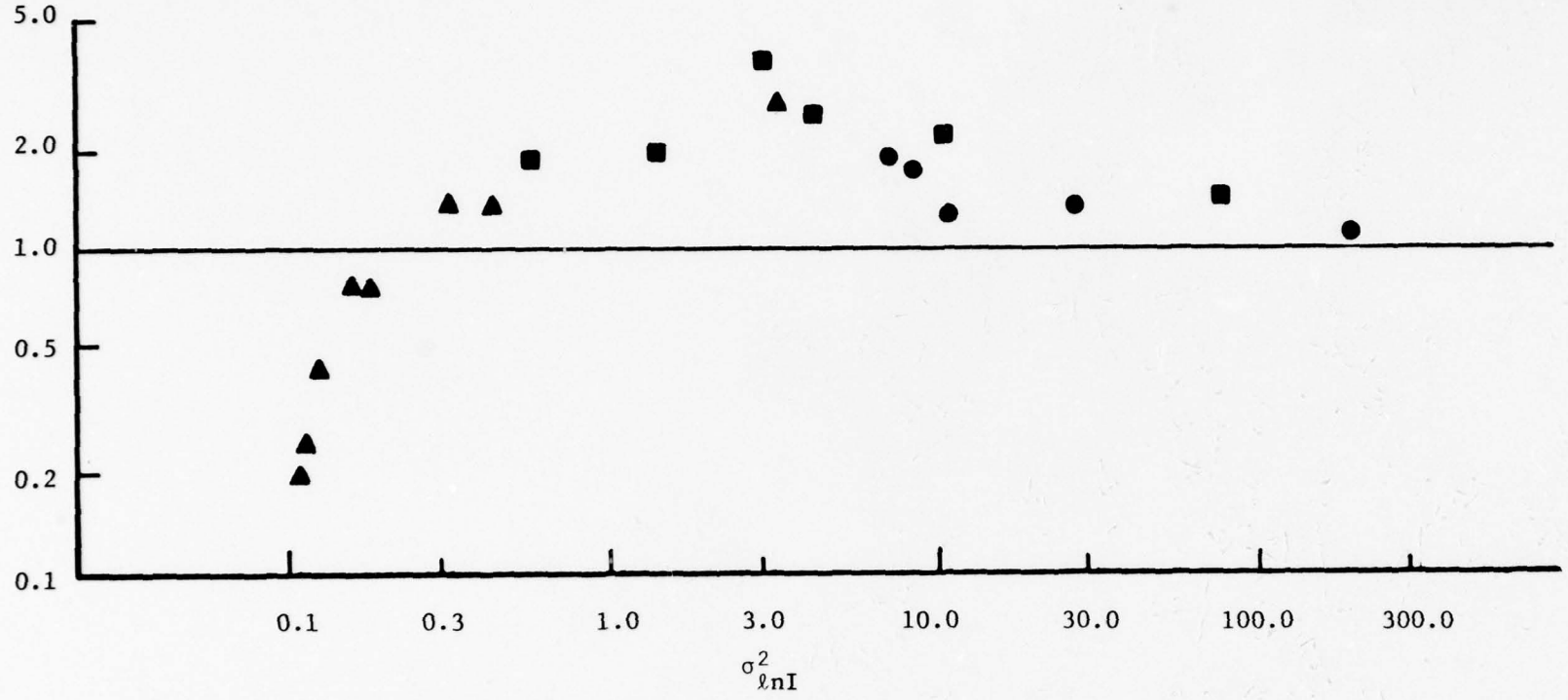

Figure 21 Normalized variance of the irradiance versus Rytov log irradiance variance.

▲ - L = 0.5 m, ■ - L = 1.5 m, ● - L = 2.5 m.

Rytov $\sigma^2_{\ell nI}$. We note the rise of $\sigma^2_{I_N}$ with turbulence level, saturation with a peak $\sigma^2_{I_N}$ of nearly 4 and a decrease back to a value near 1 at large values of $\sigma^2_{\ell nI}$. The peak value agrees well with measurements of Gurvich et al., also using ethanol. The possibility of enhanced scintillation yielding a large peak value of the normalized variance compared to that observed in the atmosphere has been predicted by Hill and Clifford.[12] This results from details of the turbulence spatial spectrum. Of course the actual optical effects will depend on the relative positions of the optical filter function, determined by $(\lambda L)^{1/2}$ and the high wave number cutoff of the turbulence spectrum, dependent on parameters of the fluid and the dissipation rate of thermal fluctuations.

Spatial covariance functions were constructed from simultaneous recordings of the irradiance at the sixteen detectors and calculation of the correlation coefficients between the various relevant pairs of detectors. Different spacings and aperture averaging effects have also been investigated by varying the magnification of the output beam before the detector array and thus varying the effective size of the individual detectors and their spacing.

A typical set of covariance curves observed at one turbulence level for three different path lengths is shown in Fig. 22. $\tilde{C}_n^2$ is approximately 8.6×10^{-11} and the observed normalized irradiance variances are L = 0.5, $\sigma^2_{I_N} = 0.72$; L = 1.5 m, $\sigma^2_{I_N} = 2.5$; L = 2.5 m, $\sigma^2_{I_N} = 1.20$. Thus this example encompasses an unsaturated condition, a nearly peak scintillation level condition and a strong saturation

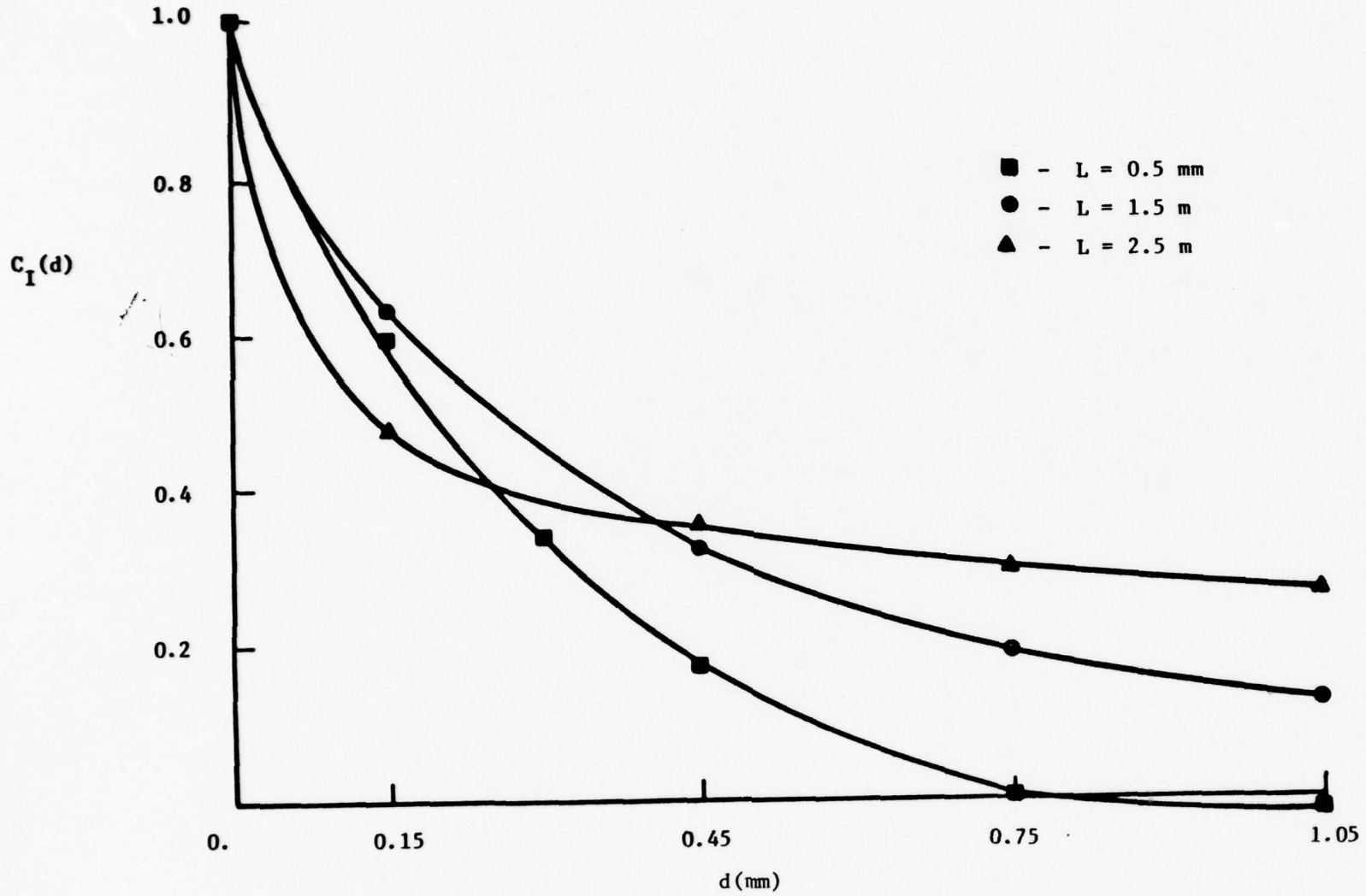

Figure 22 Spatial covariance of the irradiance. $\tilde{C}_n^2 = 8.6 \times 10^{-11}$

condition. To compare these to a first order theoretical covariance function we rescale the separation coordinate and replot the data of Fig. 22 in Fig. 23. The solid line is that obtained for a plane wave in the Rytov approximation,

$$C_I(d) = \left[\sigma^2_{\ell nI}\right]^{-1} 8\pi^2 k^2 L \int_0^\infty \left(1 - \frac{k}{\kappa^2 L} \sin \frac{\kappa^2 L}{k}\right) \psi_n(\kappa) J_o(\kappa d) \kappa \, d\kappa.$$

Here again, $\psi_n(\kappa) = (\tilde{C}_n^2/4\pi\kappa^3)(1 + \kappa\ell_1) \exp(-\kappa\ell_1)$, has been used for the spectrum. The data for all three path lengths deviate significantly from the theoretical curve with the longer path data differing by the largest amount. The deviation of the short path data is unexpected and at present we can offer no explanation. Further investigation of this problem is clearly required. We do note however that the greater path integrated turbulence cases do fall off more rapidly and approach a constant positive level which is the qualitative behavior expected. Another example is shown in Fig. 24. Here $\tilde{C}_n^2$ is approximately 2.4×10^{-10}. With this stronger turbulence level, we note the same type behavior and deviation from the theoretical curve.

We next consider the effect of receiver aperture size on the covariance function measurements. Figs. 25 and 26 show covariance functions obtained under the same turbulence conditions as seen in Fig. 24. Each figure is for a different total path length and the three curves on each figure are taken with different effective receiver aperture sizes ranging from 0.053 mm to 0.167 mm diameter.

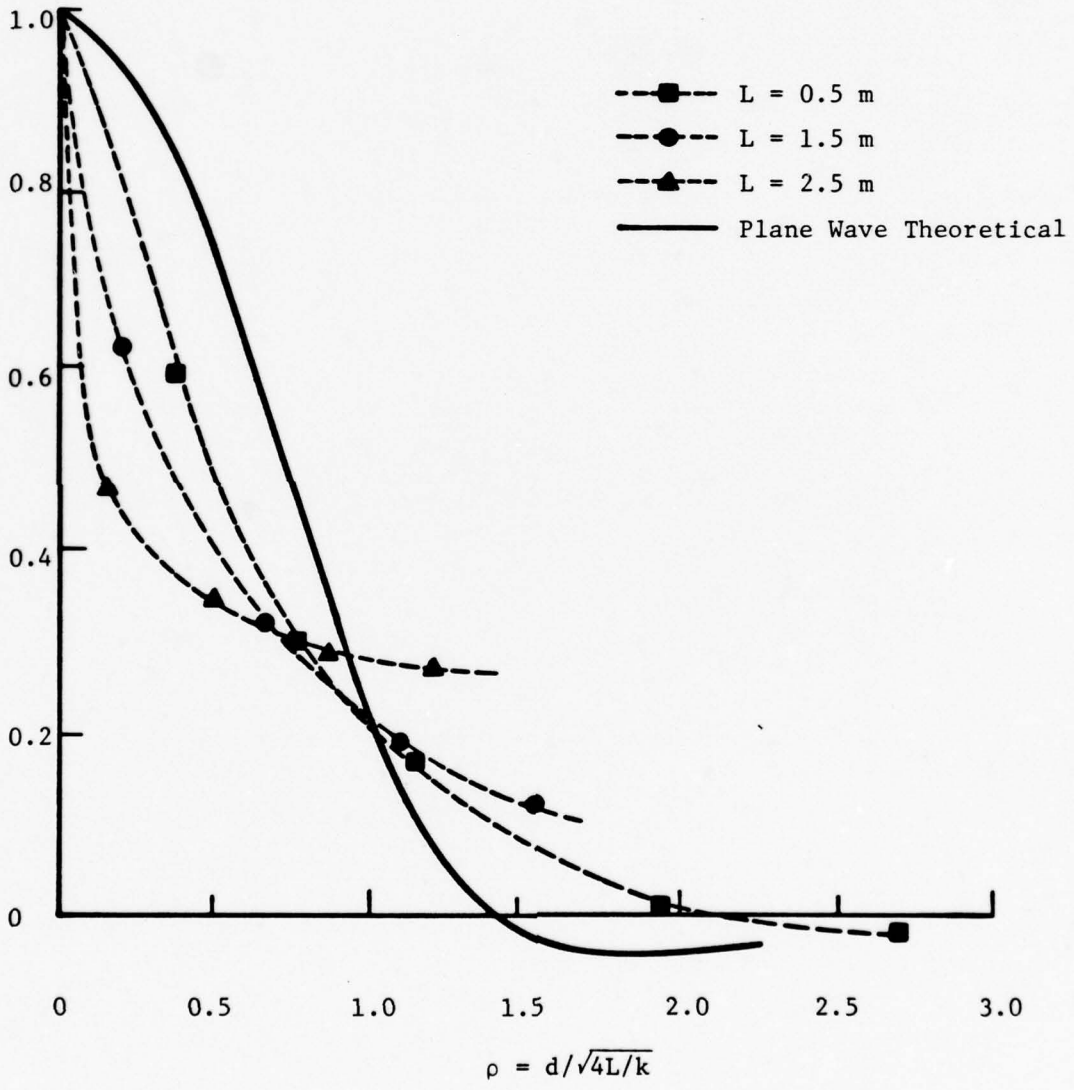

Figure 23 Spatial covariance function of the irradiance.

$\tilde{C}_n^2 = 8.6 \times 10^{-11}$

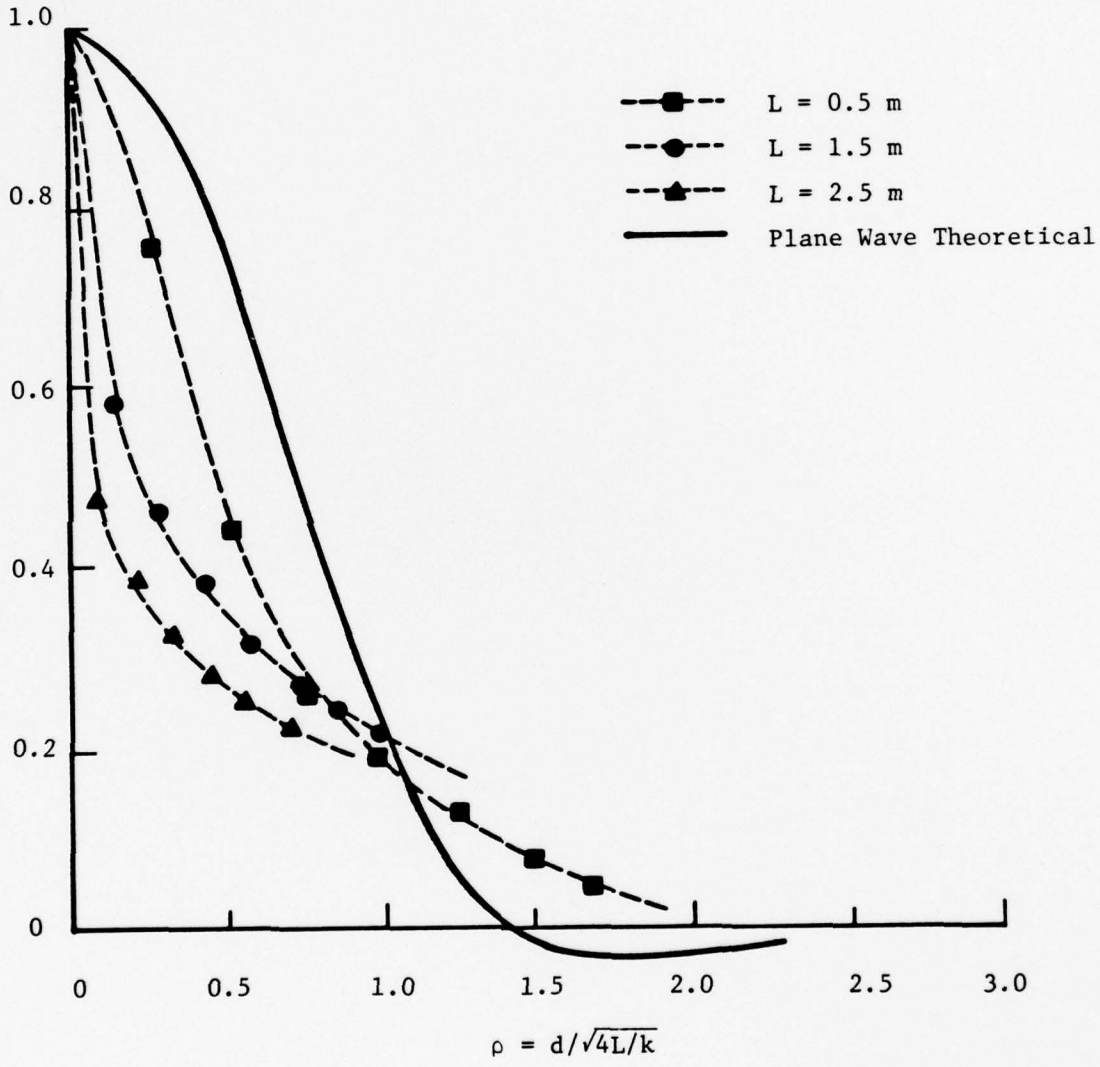

Figure 24 Spatial covariance function of the irradiance.

$\tilde{C}_n^2 = 2.4 \times 10^{-10}$

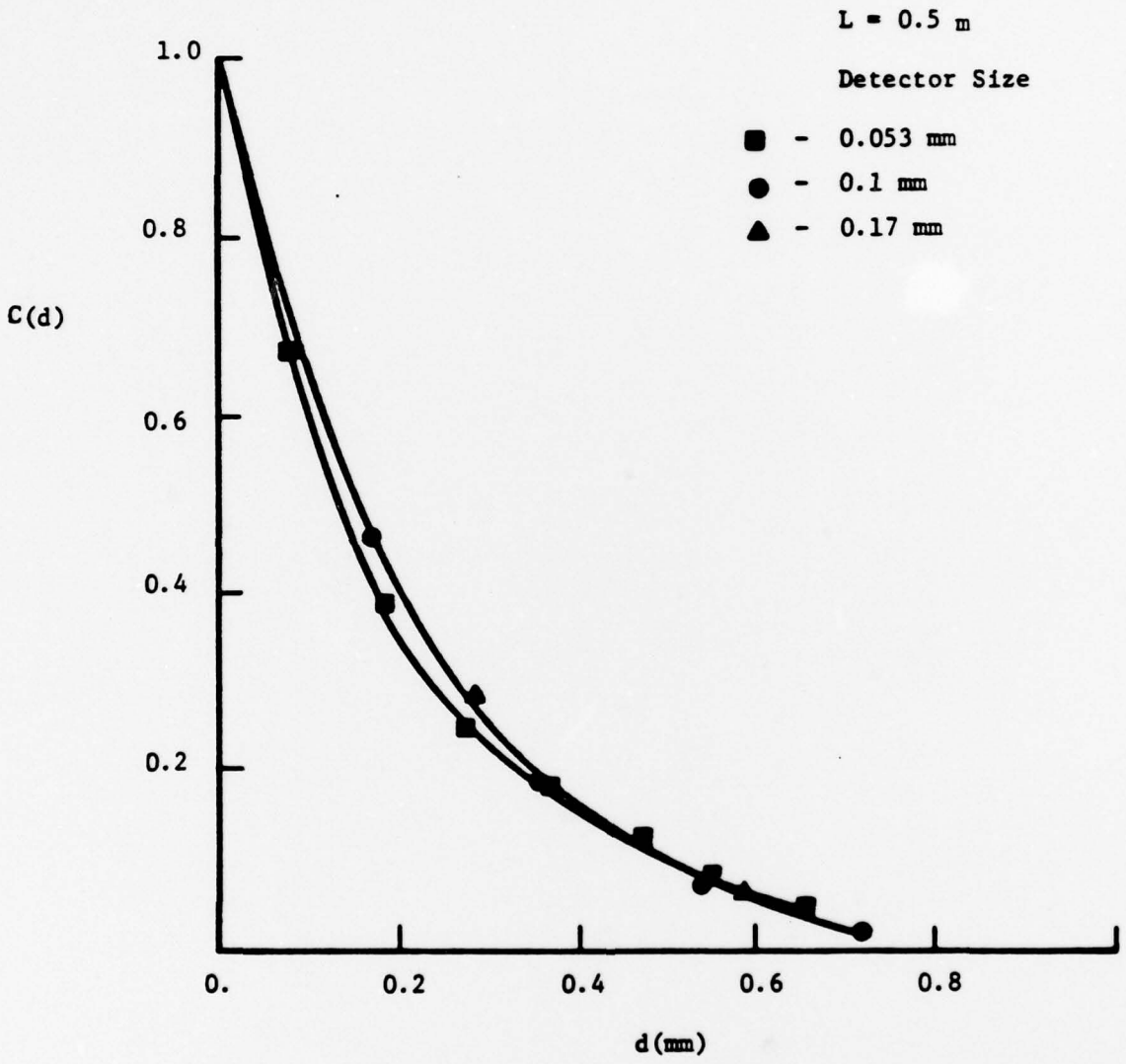

Figure 25

Spatial covariance function of the irradiance for different receiver aperture diameters. $C_n^2 = 2.4 \times 10^{-10}$. Path length 0.5 m.

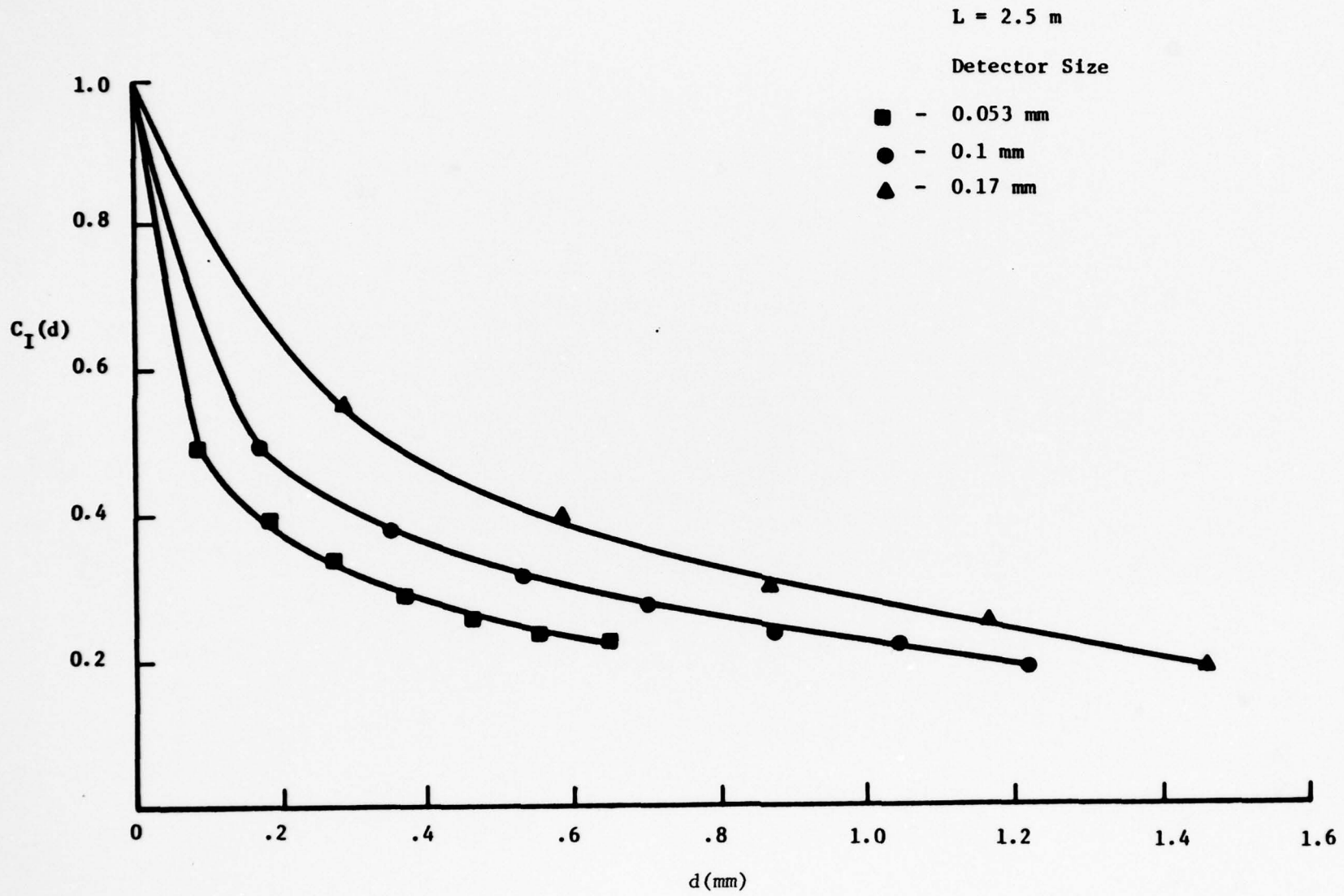

Figure 26 Spatial covariance function of the irradiance for different receiver aperture diameters. $\tilde{C}_n^2 = 2.4 \times 10^{-10}$. Path length 2.5 m.

For Fig. 25, the turbulence conditions and path length, 0.5 meters, yield unsaturated scintillation conditions. The scintillation patch size is large and the aperture sizes used in the experiment were all small compared to this patch size. Thus aperture averaging has negligible effect on the observed covariance functions. In the case of Fig. 26 L = 2.5 m and the scintillation conditions are saturated. The smallest aperture covariance function shows a rapid decrease, indicating a small covariance patch size. With increasing receiver aperture size the covariance function increases significantly indicating averaging over several scintillation patches.

One of the intentions of this work was to achieve and investigate extremely high path integrated turbulence conditions and describe the asymptotic limits of the statistical properties of the optical field in strong saturation. We have found in practice that we could reach levels of $\sigma^2_{\ell nI}$ (Rytov) of the order of 200 with reasonable path lengths. While we did not achieve as strong turbulence conditions as we would have liked, we have been able to measure a number of important statistical characteristics of the optical radiation in strong saturation. These include probability distribution functions, normalized variance and spatial covariance of the irradiance as a function of the turbulence level and path length.

III. Spherical Scatterers

We have also explored the use of a system of monodisperse spherical scatterers as a model turbulent medium. The original intent

was to use 100 μm diameter glass spheres suspended in an index matching fluid but early in this program it became evident that the uniformity and control required to simulate turbulence (very small refractive gradients) by using solid spheres in a liquid medium is uneconomical and basically impractical. We have therefore pursued an alternative approach which is novel in optical applications and which should permit the achievement of the desired scattering medium. The resultant single-scale-size scatterers are advantageous in the simplicity they lend to calculations e.g. in the multiple scattering (saturated scintillations) regime. An initial requirement, however, is to relate such a medium to the weak scattering (turbulence) regime, as follows.

Let the number of spheres of radius a per unit volume be c and the volume fraction $\phi = (4/3)\pi a^3 c << 1$. The index of refraction of the scatterers will be taken to be 1 + m and that of the surrounding medium to be 1. The mean index of refraction is then

$$\begin{aligned} \langle n \rangle &= (1 + m)\ \phi + 1 - \phi \\ &= 1 + m\phi \end{aligned}$$

and the variance in n is

$$\sigma_n^2 = \langle (n - \langle n \rangle)^2 \rangle = m^2\phi(1 - 2\phi) \approx m^2\phi$$

The correlation function of the refractive index variation

$$\gamma_n(\vec{r}_1 - \vec{r}_2) = \langle (n(\vec{r}_1) - \langle n \rangle)(n(\vec{r}_2) - \langle n \rangle) \rangle$$

may be found by calculating the probability that a rod of length $r = |\vec{r}_1 - \vec{r}_2|$ has both ends inside one of the scatterers. For dilute distributions ($\phi << 1$) this is easily effected and we obtain the well known correlation function for hard spheres

$$\gamma_n(r) = 1 - (3/2)\left(\frac{r}{2a}\right) + (1/2)\left(\frac{r}{2a}\right)^3 ; \quad 0 \leq r \leq 2a$$

$$= 0 ; \quad r > 2a$$

The spatial spectrum of index of refraction fluctuations is the 3-d Fourier transform of $\sigma_n^2 \gamma_n(r)$, i.e.

$$\psi_n(\kappa) = \frac{\sigma_n^2}{2\pi^2 \kappa} \int_0^\infty \gamma_n(r) \sin \kappa r \, r dr$$

$$= m^2 \phi \frac{3a^3}{2\pi^2} \left(\frac{j_1(a\kappa)}{a\kappa}\right)^2$$

where $j_1(x)$ is the spherical Bessel function of order 1.

The first order theory of scattering from atmospheric turbulence assumes that each scattering event is weak enough for the Born approximation to hold and that the wavelength λ << the size of a turbulent eddy. For refractive scattering from a sphere of radius a and index of refraction differing from its surroundings by m this means that $4\pi ma/\lambda << 1$ and $a >> \lambda$.

This type of scattering is commonly called Rayleigh-Debye or Rayleigh-Gans scattering. Provided these restrictions on a, λ and m are satisfied the above spatial spectrum may be freely substituted into known expressions for e.g. the variance or covariance of the log-irradiance of an initially plane wave,[2] i.e.,

$$\sigma^2_{\ell nI} = 8\pi^2 k^2 L \int_0^\infty \left(1 - \frac{k}{\kappa^2 L} \sin \frac{\kappa^2 L}{k}\right) \psi_n(\kappa) \kappa d\kappa$$

and

$$C_I(r) = 8\pi^2 k^2 L \int_0^\infty \left(1 - \frac{k}{\kappa^2 L} \sin \frac{\kappa^2 L}{k}\right) J_o(\kappa r)\ \psi_n(\kappa) \kappa d\kappa \ .$$

We find then that if the optical path length through the scattering region, $L >> \frac{2\pi a^2}{\lambda}$, the variance of the log-irradiance, $\sigma^2_{\ell nI} = 12\pi^2\ m^2 \phi a L/\lambda^2$ and the covariance

$$C_I(r) = \sigma^2_{\ell nI} \left\{ \left(1 + \frac{r^2}{8a^2}\right) \sqrt{1 - r^2/4a^2} + \frac{r^2}{4a^2} \left(1 - \frac{r^2}{16a^2}\right) \right.$$

$$\left. \times \ell n \frac{1 - \sqrt{1 - r^2/4a^2}}{1 + \sqrt{1 - r^2/4a^2}} \right\}$$

for $0 \leq r \leq 2a$ and $B_I(r) = 0$ for $r > 2a$.

This covariance curve normalized to unity is plotted in Fig. 27.

Experimental verification of this scattering theory requires a scattering medium consisting of uniformly sized spheres. The radius of these spheres must be much greater than the wavelength of the light ($a >> \lambda$) and the refractive index must differ from the intervening medium by an amount small enough to ensure that the scattering is weak ($4\pi ma/\lambda << 1$). These requirements are relatively stringent. It is difficult to control the index of refraction of materials to better than 10^{-4} which then implies, for wavelengths in the visible spectrum, that $a << 400$ μm. The optical quality of such small glass spheres is generally poor and also the densities of index matching fluids are usually much less

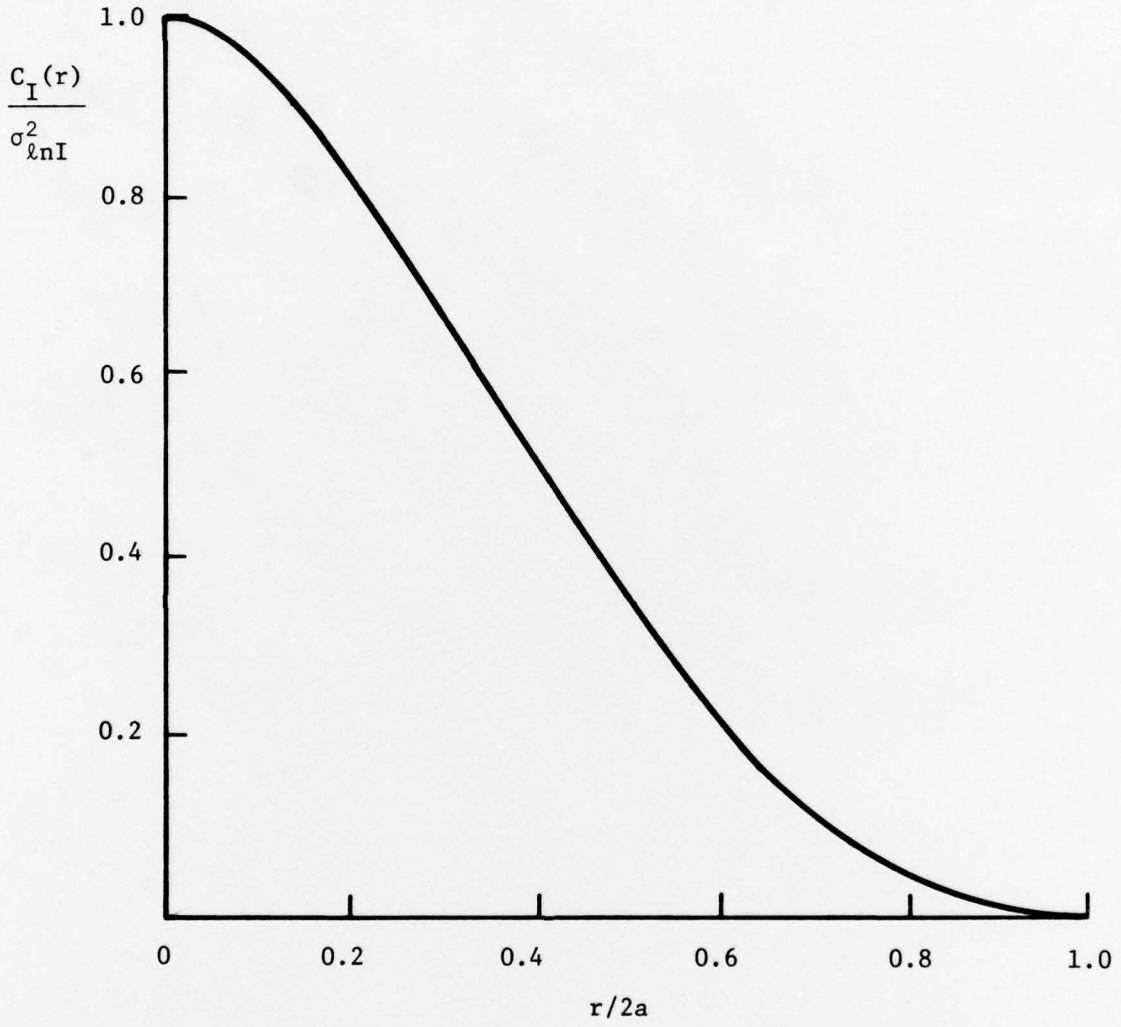

Figure 27 Covariance of irradiance for scattering from a random collection of uniform, weakly-scattering spheres of radius a.

than glass so that maintaining a distribution of glass beads in a scattering cell would be a problem. A more promising approach and the one which we have pursued is to form an emulsion of one liquid in another.

There is a large class of polymers which are soluble in water and which, when two dilute solutions are mixed together, are completely miscible but when more concentrated solutions are mixed from two distinct phases with each phase containing both polymers and water but in different concentrations. The two phases have different densities, viscosities, indices of refraction, etc. These two-phase aqueous polymer solutions have been used by biologists for separating different types of cells and certain properties of these systems have been explored.[19] However, their optical properties have not been extensively studied. We have initiated a study of one particular system to determine the feasibility of using such systems for scattering experiments.

The polymers we have initially chosen to study are polyvinyl alcohol (PVA) and Dextran. Fig. 28 shows the binodal curve for these polymers dissolved in water at 20°C. Above the curve the solution separates into two phases while for concentrations corresponding to points below the curve only one phase is present. In all cases the phases are optically clear with negligible absorption. A 5% W/W Dextran - 1.5% W/W PVA solution, for example, separates into a top (10% vol.) and bottom (90% vol.) phase, the density of the bottom phase being ~ 1.05 g/ml and that of the top

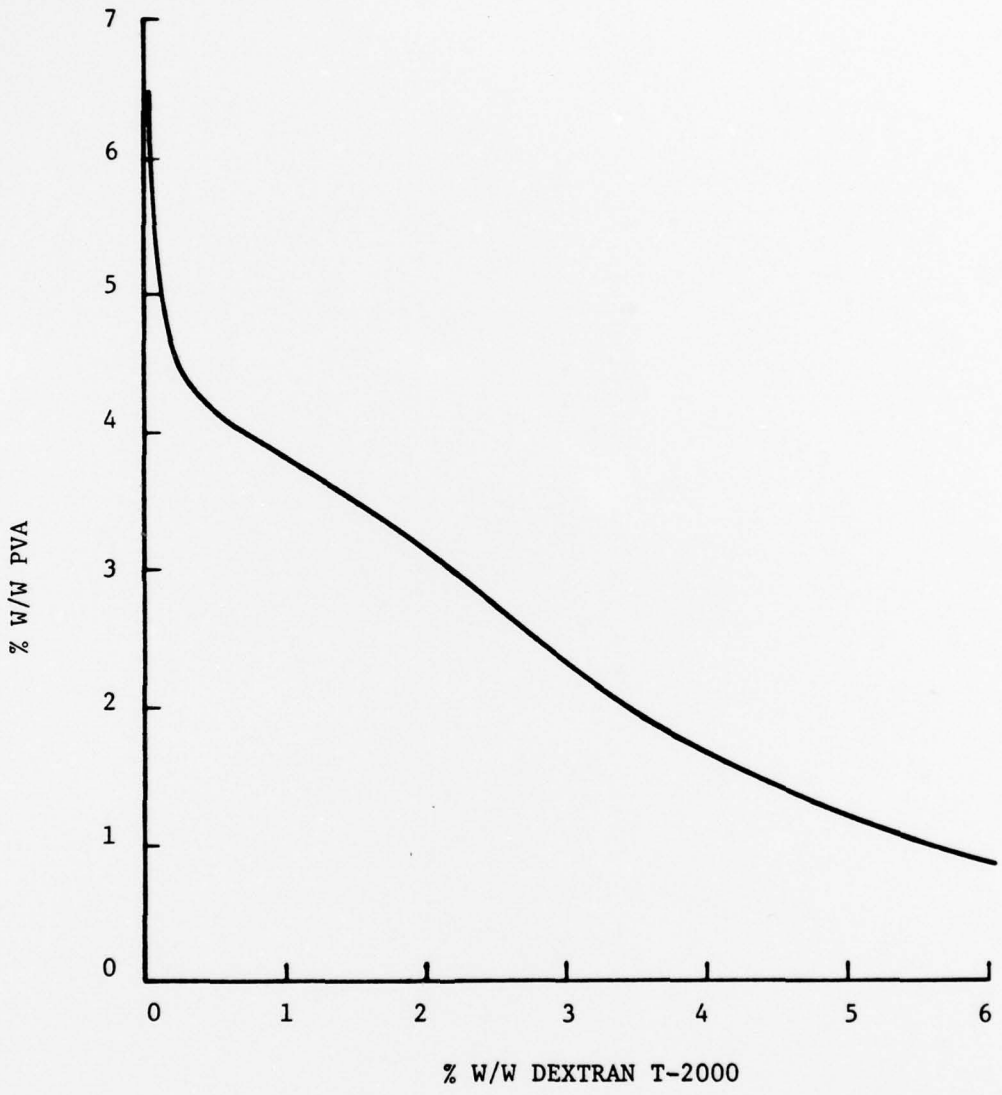

Figure 28. Binodal curve for Polyvinyl Alcohol and Dextran in water at 20°C.

through it because of the refractive scattering from the spherical droplets of the dispersed top phase. It takes several hours for the two phases to separate after an emulsion has been formed.

The emulsion has been examined microscopically and it is found to consist of a dispersion of spheres ranging in size from ~ 10 μm to 300 μm. We are currently examining methods of producing a monodisperse emulsion. One which looks promising and will be pursued involves subjecting the mixture to a constant shear for a period ranging up to an hour. This produces droplets of the dispersed phase of uniform volume.[20] The volume depends on the rate of shear, viscosity and interfacial tension. By proper choice of shear rate we expect to be able to form uniform droplets which can then be used for scattering experiments.

IV. Conclusion

A versatile and useful facility for simulating the effects of atmospheric turbulence on optical propagation has been constructed, and its parameters characterized. The strength of the turbulence generated by unstable convection has been determined as a function of power input and the structure function and spatial spectrum of the resulting index of refraction fluctuations recorded and compared with the theoretically predicted form.

The effects of this scattering medium on optical propagation has been studied in some detail. The probability density function (PDF) of the irradiance has been determined for a variety of turbulence levels and path lengths with the results conforming in

a qualitative way to the theory. The PDF does not appear to be exactly lognormal even at weak turbulence levels and short path lengths. It does appear to become progressively closer to an exponential distribution with increasing path integrated turbulence as predicted but in no case is the functional form unambiguous. Measurement of the normalized variance confirms this behavior as it approaches unity as the path integrated turbulence increases ($\sigma_{I_N}^2 = 1.09$ when the Rytov logvariance $\sigma_{\ell nI}^2 = 210$). Further work in this area should include experiments at longer path lengths and also the measured PDF should be compared with the exponential-Bessel distribution recently proposed by Bissonnette and Wizinowich.[21]

The measured spatial covariance functions of the irradiance shows considerable deviation from the first order (Rytov) theory even at weak turbulence levels which together with the deviation of the PDF from lognormal may indicate that the first order approximation is invalid sooner than expected. This should certainly be investigated in more depth and the data compared with predictions derived from the accurate multiple scattering theory.[5,6] Apart from this possible explanation there appears to be no reason for the discrepancy. Aperture averaging affects can be ruled out as they affect the covariance in the opposite manner namely the measured values would be greater than the true values. We have also determined the effects of the detector aperture size directly (see Figs. 25 and 26) and found that the

scintillation patch size was always greater than the smallest effective aperture used (53 μm).

There are of course more experiments which can be done to extend our understanding of the basic properties of the scattering medium and the effects on optical propagation particularly in the multiple scatter regime and these should be pursued. However the major use for a facility such as the one described here will probably be in the investigation of such systems and phenomena as speckle propagation through turbulence; beam wander-tracking and cancellation systems; turbulence effects on radiation reflected from glints and diffuse targets; propagation of partially coherent light; and pulse stretching. Investigations of this type will be much easier to perform, and the results will be less ambiguous because of the completely characterized scattering medium.

V. References

1. V. I. Tatarskii, Wave Propagation in a Turbulent Medium, McGraw-Hill, NY (1961).

2. R. S. Lawrence and J. W. Strohbehn, "A Survey of Clear-Air Propagation Effects Relevant to Optical Communications," Proc. IEEE 58, 1523 (1970).

3. J. R. Kerr, "Experiments on Turbulence Characteristics and Multiwavelength Scintillation Phenomena," J. Opt. Soc. Am., 62, 1040 (1972).

4. J. R. Dunphy and J. R. Kerr, "Scintillation Measurements for Large Integrated-Path Turbulence," J. Opt. Soc. Am., 63, 981 (1973).

5. H. T. Yura, "Physical Model for Strong Optical-Amplitude Fluctuations in a Turbulent Medium," J. Opt. Soc. Am., 64, 59 (1974).

6. S. F. Clifford, G. R. Ochs and R. S. Lawrence, "Saturation of Optical Scintillation by Strong Turbulence," J. Opt. Soc. Am., 64, 148 (1974).

7. M. H. Lee, R. A. Elliott, J. F. Holmes and J. R. Kerr, "Variance of Irradiance for Saturated Scintillations," J. Opt. Soc. Am., 66, 1389 (1976).

8. A. M. Prokhorov, F. V. Bunkin, K. S. Goshelashvily, and V. I. Shishov, "Laser Irradiance Propagation in Turbulent Media," Proc. IEEE, 63, 790 (1975).

9. R. L. Fante, "Electromagnetic Beam Propagation in Turbulent Media," Proc. IEEE, 63, 1669 (1975).

10. R. J. Hill, "Spectra of Fluctuations in Refractivity, Temperature, Humidity, and the Temperature-Humidity Cospectrum in the Inertial and Dissipation Ranges," J. Fluid Mech. (to be published).

11. R. J. Hill, "Optical Propagation in Turbulent Water," J. Opt. Soc. Am., 68, 1067 (1978).

12. R. J. Hill and S. F. Clifford, "Modified Spectrum of Atmospheric Temperature Fluctuations and Its Application to Optical Propagation," J. Opt. Soc. Am., 68, 892 (1978).

13. L. R. Bissonnette, "Atmospheric Scintillation of Optical and Infrared Waves: A Laboratory Simulation," Appl. Opt., 16, 2242 (1977), "Average Irradiance and Irradiance Variance of Laser Beams in Turbulent Media," Canadian Defense Research

Establishment Valcartier, Report DREV 4104/78 (1978).

14. A. S. Gurvich, M. A. Kallistratova, and F. E. Martval', "Investigation of Strong Fluctuations of the Light Intensity in a Turbulent Medium at a Small Wave Parameter," Izv. VUZ, Radiofizika 20, 1020 (1977) (in Russian).

15. J. L. Lumley and H. A. Panofsky, The Structure of Atmospheric Turbulence, p. 56, Wiley, NY (1964).

16. L. D. Landau and E. M. Lifshitz, Fluid Mechanics, p. 214, Pergamon Press, London (1959). Note that Russian authors use the term Grashof number for the Rayleigh number.

17. H. C. van de Hulst, Light Scattering by Small Particles, Wiley, NY (1957).

18. M. Kerker, The Scattering of Light and Other Electromagnetic Radiation, Academic Press, NY (1969).

19. P. A. Albertsson, Partition of Cell Particles and Macromolecules, Wiley, NY (1971).

20. A. Silberberg and W. Kuhn, J. Polymer Sci., 13, 21 (1954).

21. L. R. Bissonnette and P. L. Wizinowich, "Irradiance Probability Distribution in Saturation Regime of Optical Waves Propagating in Turbulence," Canadian Defense Research Establishment Valcartier, Report DREV 4114/78 (1978).